

The Atlantic Meridional Mode and Its Coupled Variability with the Guinea Dome

TAKESHI DOI,* TOMOKI TOZUKA, AND TOSHIO YAMAGATA

Department of Earth and Planetary Science, Graduate School of Science, The University of Tokyo, Tokyo, Japan

(Manuscript received 10 April 2009, in final form 5 August 2009)

ABSTRACT

Using an ocean–atmosphere coupled general circulation model, air–sea interaction processes associated with the Atlantic meridional mode are investigated from a new viewpoint of its link with the Guinea Dome in the northern tropical Atlantic. The subsurface thermal oceanic dome develops off Dakar from late spring to late fall owing to wind-induced Ekman upwelling. Its seasonal evolution is due to surface wind variations associated with the northward migration of the intertropical convergence zone (ITCZ). Since the upwelling cools the mixed layer in the Guinea Dome region during summer, it is very important to reproduce its variability in order to simulate the sea surface temperature (SST) there.

During the preconditioning phase of the positive (negative) Atlantic meridional mode, the dome is anomalously weak (strong) and the mixed layer is anomalously deep (shallow) there in late fall. This condition reduces (enhances) the sensitivity of the mixed layer temperature to the climatological atmospheric cooling. As a result, the positive (negative) SST anomaly appears there in early winter. Then, it develops in the following spring through the wind–evaporation–SST (WES) positive feedback associated with the anomalous northward (southward) migration of the ITCZ. This, in turn, leads to the stronger (weaker) Ekman upwelling and colder (warmer) subsurface temperature in the dome region during summer. It plays an important role on the decay of the warm (cold) SST anomaly through entrainment as a negative feedback. Therefore, simulating this interesting air–sea interaction in the Guinea Dome region is critical in improving prediction skill for the Atlantic meridional mode.

1. Introduction

The Atlantic meridional mode (AMM) is a climate mode associated with the cross-equatorial meridional gradient of the sea surface temperature anomaly (SSTA) in the tropical Atlantic. It is sometimes referred to as the gradient mode or the Atlantic dipole mode [see Xie and Carton (2004) for a recent review on the AMM] and plays important roles in interannual and decadal climate variations. Because the AMM is associated with the anomalous meridional migration of the intertropical convergence zone (ITCZ), it has a significant impact on rainfall over the tropical Atlantic, especially over north-

eastern Brazil and the Sahel region (Kushnir et al. 2006). Also, the AMM is closely linked with the hurricane activity that causes severe disasters in the United States and neighborhood countries (Xie et al. 2005; Vimont and Kossin 2007; Kossin and Vimont 2007). Thus, understanding its mechanism is important from a societal viewpoint.

The AMM was originally identified by Servain (1991) using a principal component analysis. The evolution of the coupled mode is locked to boreal spring and develops through thermodynamic air–sea interaction linked with the ITCZ migration; weaker (stronger) trade winds in the Northern Hemisphere associated with the anomalously northward (southward) shift of the ITCZ are responsible for warming (cooling) SSTA there by suppressing (intensifying) evaporation and thus latent heat loss. This process is known as the wind–evaporation–SST (WES) positive feedback (Carton et al. 1996; Chang et al. 1997; Xie 1999).

Although many studies on the AMM have been carried out, most of them focused on the atmospheric forcing of the SSTA and remote influences from the ENSO and the North Atlantic Oscillation, and paid little

* Current affiliation: Application Laboratory/Japan Agency for Marine–Earth Science and Technology, 3173-25 Syouwa-chou, Kanazawa-ku, Yokohama, Kanagawa 236-0001, Japan.

Corresponding author address: Takeshi Doi, 3173-25 Syouwa-chou, Application Laboratory/Japan Agency for Marine–Earth Science and Technology, Kanazawa-ku, Yokohama, Kanagawa 236-0001, Japan.
E-mail: tdoi@jamstec.go.jp

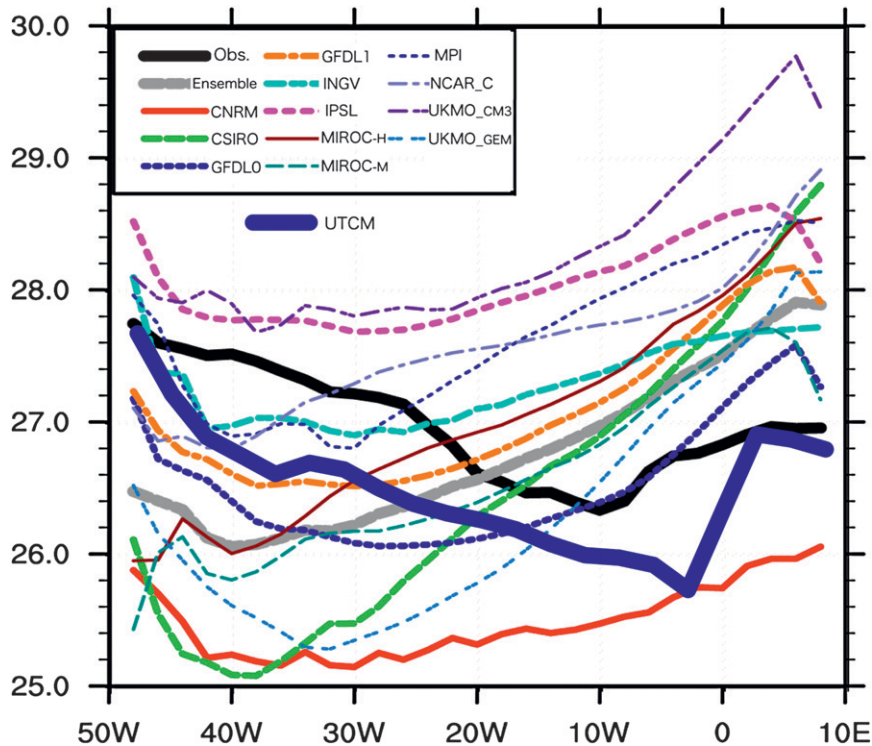


FIG. 1. Annual mean SST ($^{\circ}\text{C}$) along the equator averaged between 2°S and 2°N from selected CMIP3 models (adopted from Richter and Xie 2008). ICOADS observations are shown by thick black line. UTCM is superimposed by thick indigo blue line.

attention to its link with the in situ subsurface upwelling dome. However, Doi et al. (2009) have pointed out a close connection between the AMM and an oceanic thermal upwelling dome in the northeastern tropical Atlantic, which is known as either the Dakar Dome or the Guinea Dome (GD) (Rossignol and Meyrueis 1964; Mazeika 1967). It may play an important role in determining the SST there through the heat transport associated with variations of the thermocline depth. However, the detailed air–sea interaction involving the GD remains unclear as this previous work used a stand-alone ocean general circulation model. Therefore, we investigate the air–sea interaction process in the GD region and its link with the AMM using an ocean–atmosphere coupled general circulation model (CGCM) for the first time.

The content is organized as follows. In section 2, descriptions of our coupled model and its validation are given. We discuss how the zonal SST gradient along the equatorial Atlantic is simulated well in our model, in contrast with many other CGCMs. In section 3, simulated seasonal variations of the GD and its air–sea interaction are investigated. The air–sea coupled process associated with the AMM and its link with interannual variability of the GD are discussed in section 4. The final section is reserved for summary and discussions.

2. Model

a. Description

The CGCM used in this study is the University of Tokyo Coupled General Circulation Model (UTCM) (Chakraborty et al. 2003; Tozuka et al. 2006). The oceanic component is the Modular Ocean Model, version 3 (MOM3) (Pacanowski and Griffies 2000). It covers a near-global ocean from 65°S to 65°N . The horizontal grid space in the meridional direction varies from 0.5° between 20°S and 20°N to 2° near 65°S and 65°N , while that in the zonal direction is held constant at 2.8125° . There are 25 vertical levels with 9 levels in the upper 110 m. The bottom topography is adopted from the 5' Earth topography (ETOPO5) dataset. Lateral viscosity and diffusivity are based on the formula given by Smagorinsky (1963). Also, the Gent and McWilliams (1990) parameterization is adopted to incorporate effects of mesoscale eddies. The parameterization of Pacanowski and Philander (1981) is adopted for the vertical mixing. In the sponge layer within 5° from northern and southern artificial boundaries, the temperature and salinity fields are restored to monthly mean climatological values [*World Ocean Atlas 1998* (WOA98; Conkright et al. 1998)] at all depths.

TABLE 1. Summary of model biases during boreal spring. (a) Location of ITCZ ($^{\circ}$), defined as zero meridional wind stress averaged between 30° and 20° W; QuickSCAT data used as the reference. (b) SLP (hPa) over northeastern Brazil (10° S– 10° N, 70° – 50° E); NCEP–NCAR reanalysis data used as reference. (c) Southerly wind stress (N m^{-2}) averaged over southeastern Atlantic (10° S– 0° , 5° – 10° E); QuickSCAT data used as reference. (d) Meridional SLP difference (hPa) for southeastern equatorial coastal region (10° S– 0° , 5° – 10° E) minus eastern Sahel region (5° – 15° N, 5° – 10° E); NCEP–NCAR reanalysis data used as reference.

	(a) Location of ITCZ	(b) SLP over Brazil	(c) Southerly wind stress	(d) Meridional SLP difference
Observation (reference)	2.0°N	1011.2	0.036	2.4
UTCM (our model)	+2.8	–1.6	–0.010	0.0
Centre National de Recherches Météorologiques Coupled Global Climate Model, version 3 (CNRM-CM3)	–8.7	+0.9	–0.031	–1.55
Commonwealth Scientific and Industrial Research Organisation Mark version 3.0 (CSIRO Mk3.0)	–4.8	+1.1	–0.031	–1.1
GFDL CM2.0	–0.5	–0.1	–0.026	–0.9
GFDL CM2.1	–2.3	–1.1	–0.028	–1.2
Istituto Nazionale di Geofisica e Vulcanologia (INGV)-SXG	–4.7	–0.4	–0.025	–1.6
IPSL CM4	–1.2	–1.0	–0.023	–0.3
MIROC3.2(hires)	–0.5	+0.2	–0.024	–1.7
MIROC3.2(medres)	+3.5	+1.0	–0.017	–1.4
Max Planck Institute Ocean Model (MPI-OM)	–4.7	+0.4	–0.026	–1.8
NCAR Community Climate System Model, version 3 (CCSM3)	–4.7	+1.0	–0.036	–2.9
HadCM3	–1.3	–2.1	–0.038	–0.6
Hadley Centre Global Environmental Model version 1 (HadGEM1)	–4.8	+0.1	–0.016	–0.5

The atmospheric component is the Frontier Atmosphere Model, version 1.1 (FrAM) and its details are given in Guan et al. (2000). It has triangular truncation at wavenumber 42 (T42, corresponding to 2.8125°) in the horizontal, and there are 28 hybrid vertical levels from the surface up to the 10-hPa level. The land surface model in UTCM is based on the model of Viterbo and Beljaars (1995). The penetrative deep convection scheme of Kuo (1974) is used with a little modification. FrAM simulates not only the Asian summer monsoon climatology (Guan et al. 2000), but also the regional influences of climate variability associated with the Indian Ocean dipole (IOD) and ENSO (Chakraborty et al. 2006). The model is spun up for 10 years using monthly climatology of the Global Sea Ice and Sea Surface Temperature (GISST) dataset and Gridded Sea Ice Information (SIGRID) dataset (available online at http://nsidc.org/data/docs/daac/nsidc0050_aari_seaice/sigrid.html) from an isothermal condition without motion. Then, FrAM and MOM3 are coupled and integrated for 100 years with the UTCM coupler developed by Chakraborty et al. (2003). Fluxes are exchanged daily; no flux adjustment is taken between 60° S and 60° N. This simulation corresponds to a present-day control experiment. We have calculated monthly climatologies by averaging the model monthly mean output for the last 70 years. In section 4, we focus on the interannual variation of the AMM rather than its decadal variability (cf. Chang et al. 1997). Therefore, we define anomaly fields as deviations from the monthly mean climatology for the last 70 years, after removing

variability beyond a period of 8 yr using a high-pass wavelet filter (Torrence and Compo 1998). Also, a 3-month running mean is applied.

For comparison with the observation, we use the subsurface temperature data from the *World Ocean Atlas 2005* (WOA05; http://www.nodc.noaa.gov/OC5/WOA05/pr_woa05.html). Also, we use the Quick Scatterometer (QuickSCAT) data for wind stress data (Kubota et al. 2002) and the Extended Reconstructed SST, version 2 (ERSSTv2) data for SSTA (Smith and Reynolds 2004). For the 2005 positive AMM event, we use the subsurface temperature data from the Prediction and Research Moored Array in the Atlantic (PIRATA) (Bourles et al. 2008), Japan Agency for Marine–Earth Science and Technology (JAMSTEC)/Institute of Observational Research for Global change (IORGC) Argo data (http://www.jamstec.go.jp/ARGO/J_ARGOe.html), and the Visible Infrared Scanner (VIRS) SST data for SSTA (http://www.eorc.jaxa.jp/TRMM/imgdt/day_vrs/readme1.htm).

b. Validation for the zonal SST gradient

Many CGCMs suffer from serious biases in the tropical Atlantic (Davey et al. 2002). In particular, as shown in Fig. 1, almost all Coupled Model Intercomparison Project phase 3 (CMIP3) (Meehl et al. 2007) models show the zonal SST gradient along the equator opposite to the observation (Richter and Xie 2008). Lack of the cold tongue in the equatorial Atlantic may be the major reason why many CGCMs fail to simulate and predict the Atlantic Niño (Stockdale et al. 2006), which

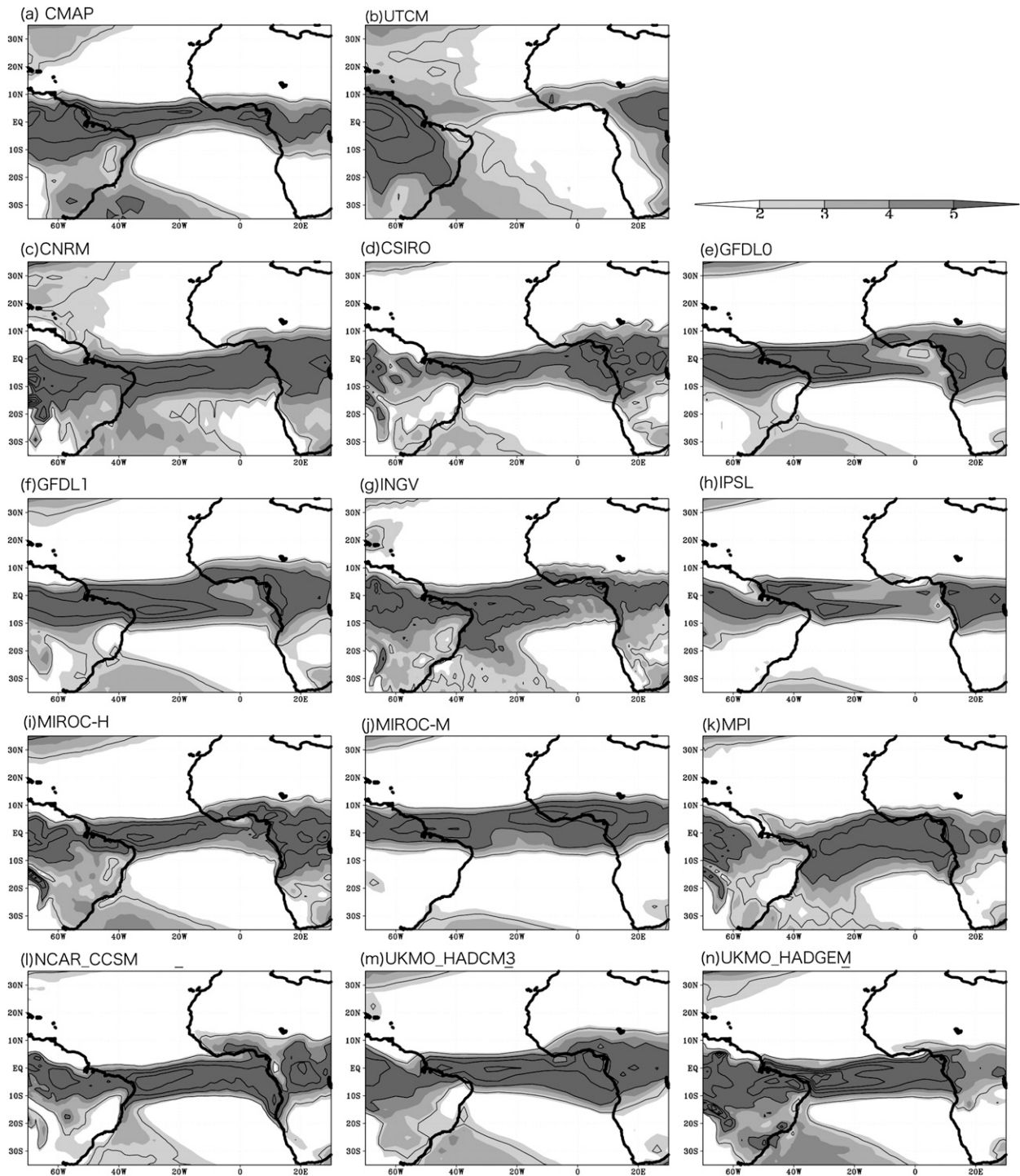


FIG. 2. Precipitation (mm day^{-1}) in boreal spring (Mar–May) from (a) CMAP (Xie and Arkin 1997), (b) UTCM, and (c)–(n) selected CMIP3 models. Contour interval is 2.5 mm day^{-1} .

is one of the major interannual climate modes in the tropical Atlantic (Zebiak 1993). In contrast to CMIP3 models, UTCM simulates the zonal gradient of SST along the equator surprisingly well (Fig. 1). These an-

nual mean features become more prominent in boreal summer when the cold tongue reaches its seasonal maximum. UTCM is successful in simulating this development of the cold tongue in boreal summer, whereas

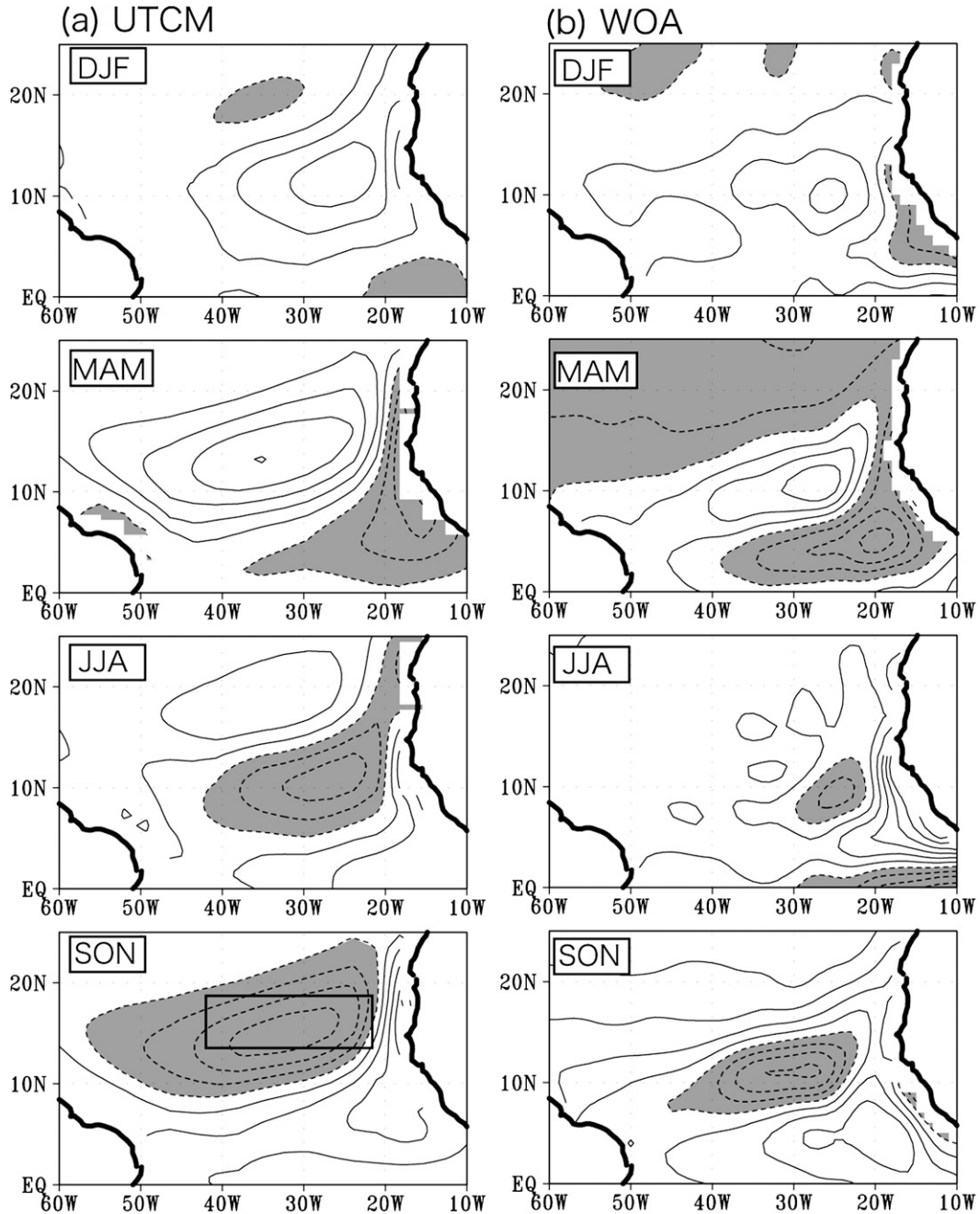


FIG. 3. (a) Annual march of deviation from annual mean of subsurface temperature at a depth of 105 m from UTCM. (b) Same as (a), but for a depth of 50 m in WOA05. Contour interval is 0.5°C. Temperature deviation lower than -0.5°C is shaded. Location of Region A (14°–18°N, 42°–22°W) is also shown for SON in (a).

almost all CMIP3 models failed in this aspect (figure not shown).

Using composites of the CMIP3 models, Richter and Xie (2008) suggested that this bias originates from weaker easterlies along the equator as the ITCZ is displaced to the south of the observed latitude during boreal spring. Table 1a shows the location of the sim-

ulated ITCZ defined by the zero meridional wind stress line in boreal spring. The ITCZ in UTCM is located to the north of the observation, in contrast with most CMIP3 models. This may partly explain why UTCM can capture the amplitude of the easterly trade winds and the zonal gradient of SST along the equator. However, the Model for Interdisciplinary Research on

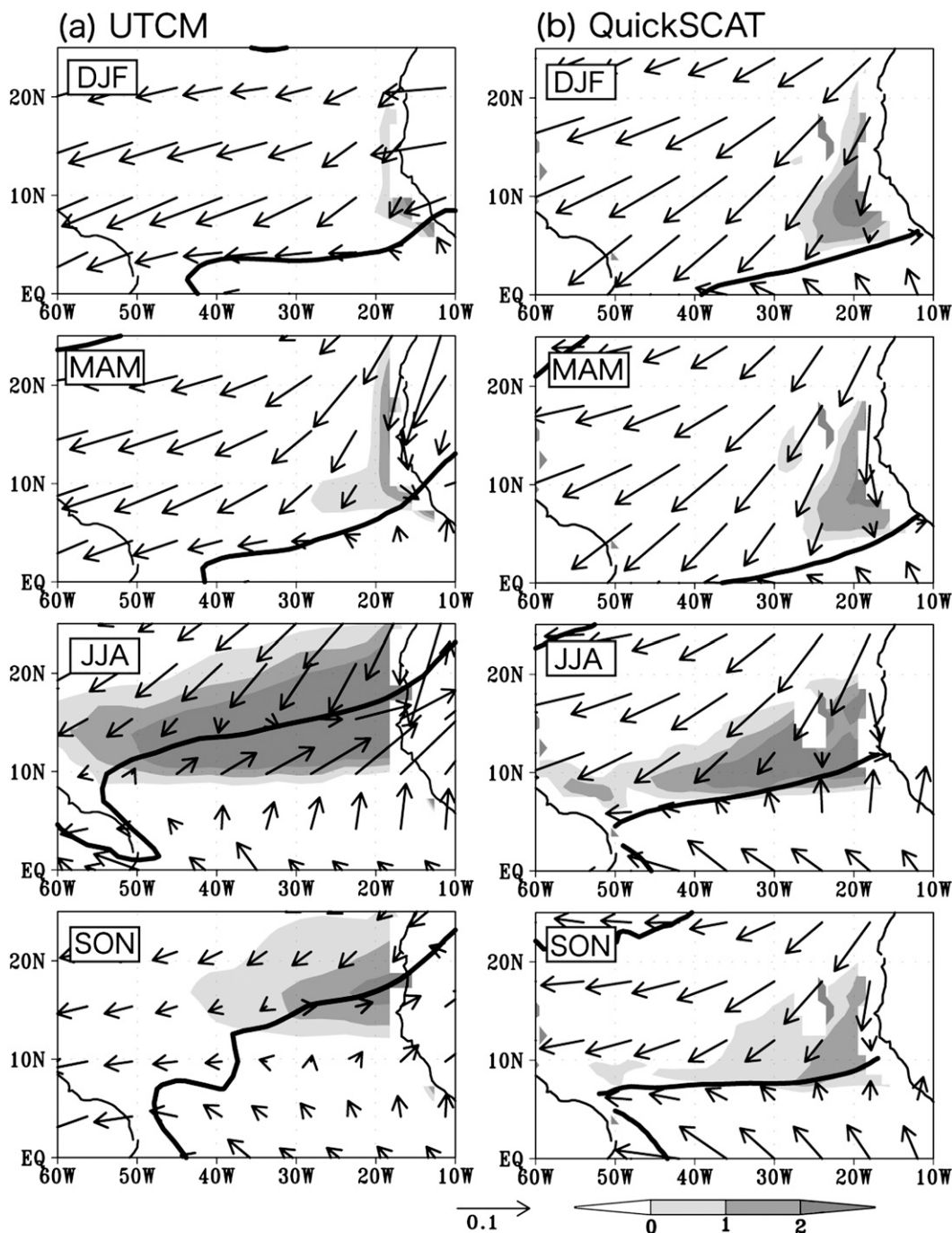


FIG. 4. Annual cycle of wind stress (N m^{-2} ; vector) and Ekman upwelling (10^{-6} m s^{-1} ; shaded) from (a) UTCM and (b) QuickSCAT. Also, location of the ITCZ, defined as zero meridional wind stress, is shown (thick line).

Climate 3.2, medium-resolution version MIROC3.2 (medres) cannot simulate the zonal gradient of SST, even though the ITCZ is located to the north of that in UTCM. Also, locations of the ITCZ in some models {Geophysical Fluid Dynamics Laboratory Climate Model version 2.0 (GFDL CM2.0), Model for Interdis-

ciplinary Research on Climate 3.2, high-resolution version [MIROC3.2(hires)], L'Institut Pierre-Simon Laplace Coupled Model, version 4 (IPSL CM4), and the third climate configuration of the Met Office Unified Model (HadCM3)} are in agreement with the observation, but these models fail to reproduce the zonal SST gradient.

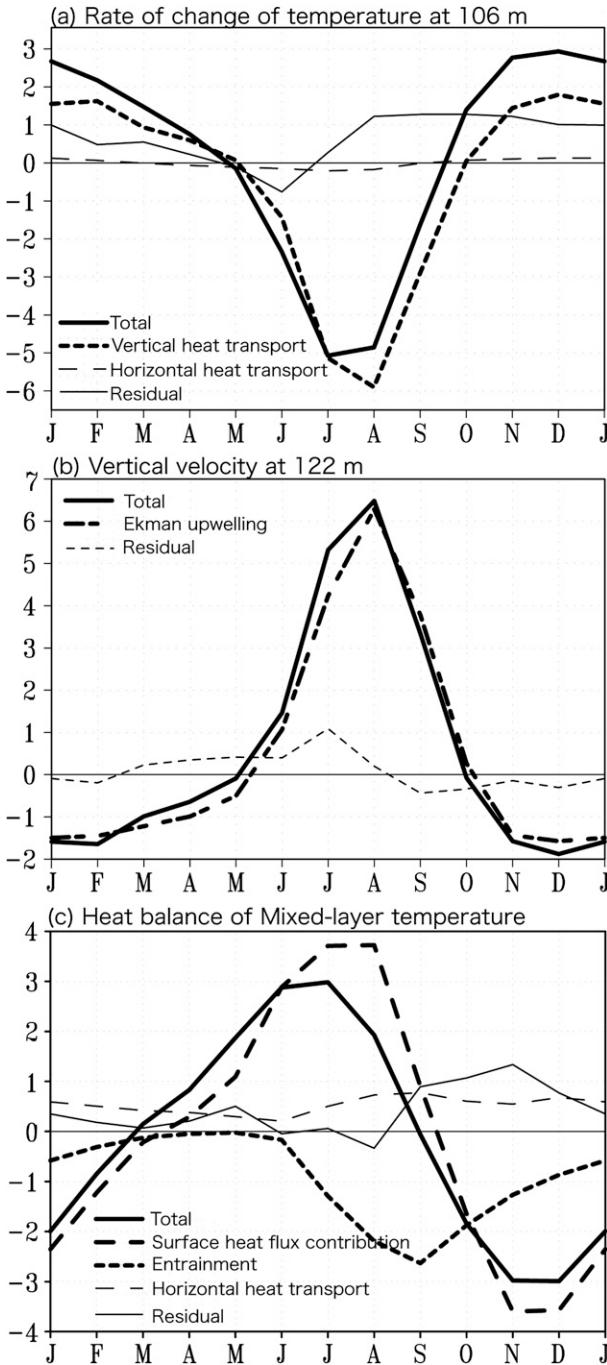


FIG. 5. (a) Heat balance of temperature at a depth of 106 m for Region A (10^{-7} K s^{-1}). Rate of change (“Total”) is determined by vertical heat transport, horizontal heat transport, and residual. (b) Vertical velocity at a depth of 122 m (10^{-6} m s^{-1}) for Region A: modeled vertical velocity (“Total”) is determined by regional wind-induced Ekman upwelling and residual. (c) Heat balance of mixed layer temperature for Region A (10^{-7} K s^{-1}): rate of change (“Total”) is determined by sea surface heat flux contribution, oceanic cooling associated with entrainment, oceanic horizontal heat transport, and residual [see Eq. (1)].

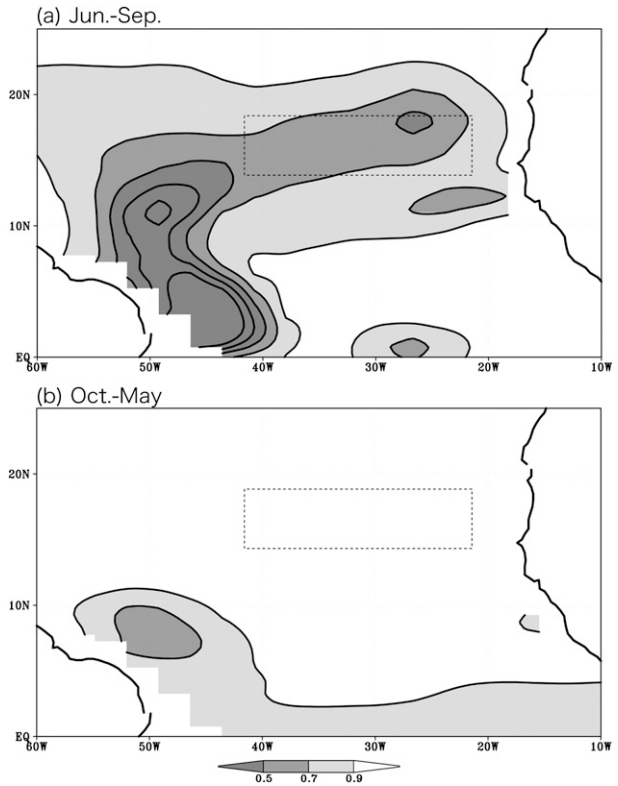


FIG. 6. Correlation coefficient between the climatological rate of change of mixed layer temperature [first term on lhs of Eq. (1)] and the climatological sea surface heat flux contribution [first term on rhs of Eq. (1)] (a) from June to September and (b) from October to May: Contour interval 0.2; values lower than 0.9 shaded. Location of Region A (14° – 18° N, 42° – 22° W) is also shown by dashed line.

Therefore, we need to seek another major reason for those models.

The sea level pressure (SLP) and wind stress in boreal spring is crucial for simulating the cold tongue in boreal summer. The low SLP over the South American continent is closely linked with the easterly in the western equatorial region. Although the low SLP near northeastern Brazil is underestimated in most of the CMIP3 models more than in the observation, UTCM and three CMIP3 models [GFDL Coupled Model, version 2.1 (CM2.1), IPSL CM4, and HadCM3] simulate the low SLP there too strongly, as shown in Table 1b. However, GFDL CM2.1 and HadCM3 cannot simulate the reasonable strength of the easterly because of anomalously lower SLP over the African continent (figure not shown).

The low SLP over the African continent also influences southerly winds in the southeastern tropical Atlantic, which induce upwelling along the West African coast in the Southern Hemisphere. The cold upwelled water then extends westward by advection and Rossby

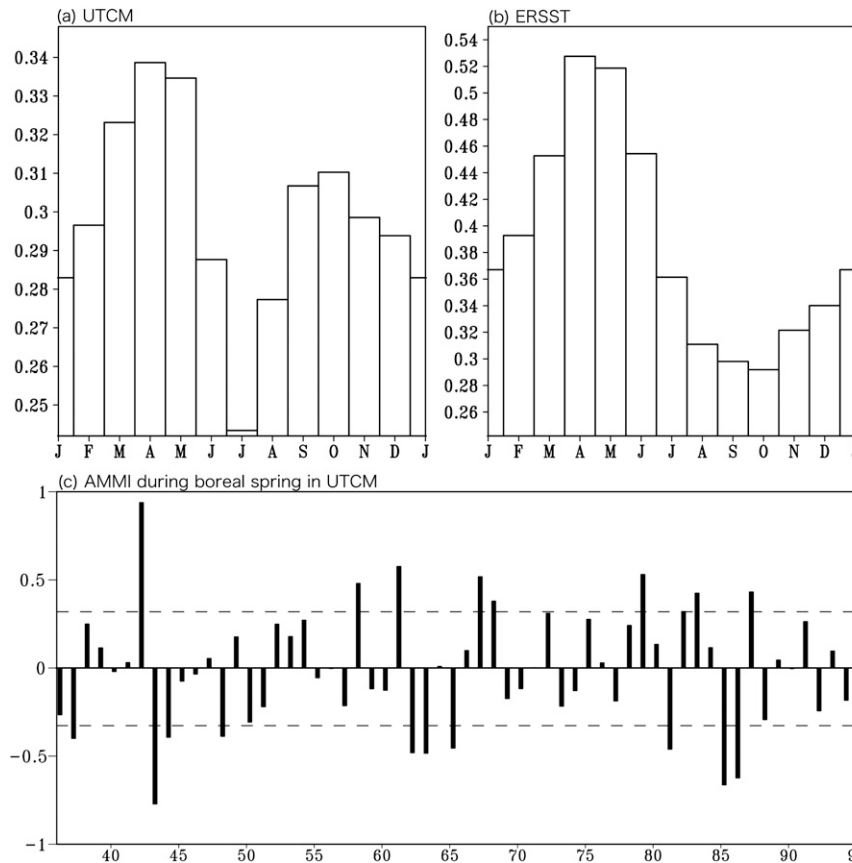


FIG. 7. (a) Monthly standard deviation of the Atlantic meridional mode index (AMMI) defined as SSTA averaged in the northern region (5° – 15° N, 50° – 20° W) minus that in the southern region (5° – 15° S, 20° W– 10° E) for UTCM ($^{\circ}$ C). (b) As in (a) but for ERSSTv2. (c) Spring AMMI by averaging the AMMI from March to May in UTCM ($^{\circ}$ C).

wave propagation and causes the cold SST in the eastern equatorial region (Philander and Pacanowski 1981). Table 1c shows the southerly wind stress averaged in the equatorial coastal region (10° S– 0° , 5° – 10° E). UTCM simulates 70% of the observed strength of southerly wind stress, while it is less than 50% in almost all CMIP3 models. GFDL CM2.0, MIROC3.2(hires), and IPSL CM4 capture only 30%, even though the location of the ITCZ is well simulated. The coastal southerly wind in MIROC3.2(medres) is only about 50% of the observation, although the ITCZ is located farther northward. Therefore, not only the location of the ITCZ, but also the strength of southerly wind near the coast, is crucial in simulating the realistic zonal SST gradient. This supports Hazeleger and Haarsma (2005), who showed that the coastal upwelling in the southeastern tropical Atlantic is important for reducing the zonal SST bias, using the sensitivity experiment of entrainment efficiency. Also, Hu et al. (2008) suggested that it is critical for this bias to simulate the cross-equatorial meridional wind associated with the African monsoon. In fact, the me-

ridional SLP gradient between the eastern Sahel region (5° – 15° N, 5° – 10° E) and the southeastern equatorial coastal region (10° S– 0° , 5° – 10° E) in UTCM is in agreement with the observation, in contrast with almost all CMIP3 models (Table 1d).

Furthermore, almost all of the CMIP3 models overestimate the precipitation over the southeastern equatorial Atlantic in boreal spring, while UTCM underestimates the precipitation there (Fig. 2). As pointed out by Breugem et al. (2008), the excess in precipitation leads to a spurious barrier layer in the southeastern equatorial Atlantic. Since the barrier layer significantly contributes to the warm SST bias by suppressing the efficiency of cold-water entrainment, it provides a favorable condition for UTCM to simulate cold SST in the east. Also, the precipitation over northeastern Brazil is overestimated in UTCM compared with the CMIP3 model outputs, which may be linked with the reasonable strength of the easterly in the western equatorial region. This is consistent with the anomalously lower SLP over northeastern Brazil in UTCM, as shown in Table 1b. Since

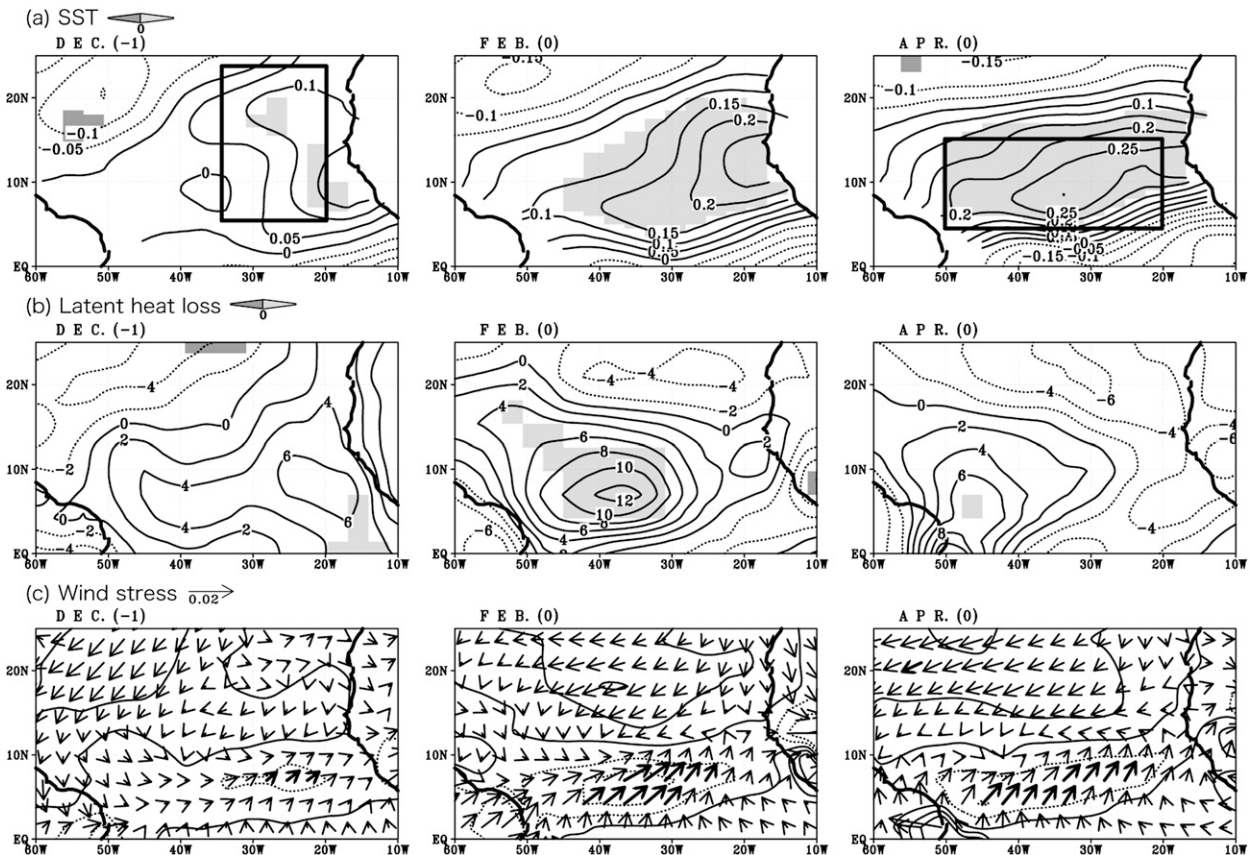


FIG. 8. Composite anomalies for the positive AMM years. (a) SST anomaly. Contour interval is 0.05°C . Locations for the heat budget analysis ($5^{\circ}\text{--}24^{\circ}\text{N}$, $36^{\circ}\text{--}20^{\circ}\text{W}$, and $5^{\circ}\text{--}15^{\circ}\text{N}$, $50^{\circ}\text{--}20^{\circ}\text{W}$) are also shown for December (–1) and April (0). (b) Latent heat loss anomaly: positive value means that it warms ocean. Contour interval is 2 W m^{-2} . (c) Wind stress anomaly: vector shows wind stress anomaly and contour shows strength anomaly of wind stress, interval 0.005 N m^{-2} . 0 indicates the AMM years and –1 the previous years. Light (dark) shading denotes positive (negative) anomalies above 90% significance level in (a) and (b); in (c) anomalies above 90% significance level shown by thick arrows.

small biases may evolve owing to false air–sea–land coupled processes, we need further efforts to improve coupled models.

In this subsection, we have shown that the present model, compared to almost all CMIP3 models, has better skill in the tropical Atlantic. From the next section, we focus on our main purpose: the air–sea coupled process in the GD region and its link with the AMM. Validations directly related to the GD and the AMM are shown in each section.

3. Annual cycle

The seasonal variation of the GD is simulated rather well in UTCM. Figure 3 shows the annual march of the deviation from annual mean of subsurface temperature. As the simulated thermocline is deeper by about 50 m than the observation, we compare the simulated subsurface temperature at a depth of 105 m with the sub-

surface temperature of *WOA05* at a depth of 50 m. As shown in Fig. 3, the simulated cold subsurface temperature develops during boreal summer and reaches the coldest temperature in boreal fall. Its annual cycle is due to intensified Ekman upwelling associated with the northward shift of the ITCZ, as seen in Fig. 4. The annual cycle of wind stress is very similar to the observation except that the simulated ITCZ shifts too far north by a few degrees from spring through fall. This is why the simulated GD is located north of the observed position.

To understand the annual cycle of the GD quantitatively, we introduce an artificial “Region A” ($14^{\circ}\text{--}18^{\circ}\text{N}$, $42^{\circ}\text{--}22^{\circ}\text{W}$; see Fig. 3) that includes most of the developed dome in fall. From the vertical distribution of the rate of change of climatological temperature in Region A (figure not shown), it is identified that the subsurface cooling in summer is out of phase with sea surface heating. This simulated feature is very similar to the observation, although it is about 50 m deeper. The seasonal

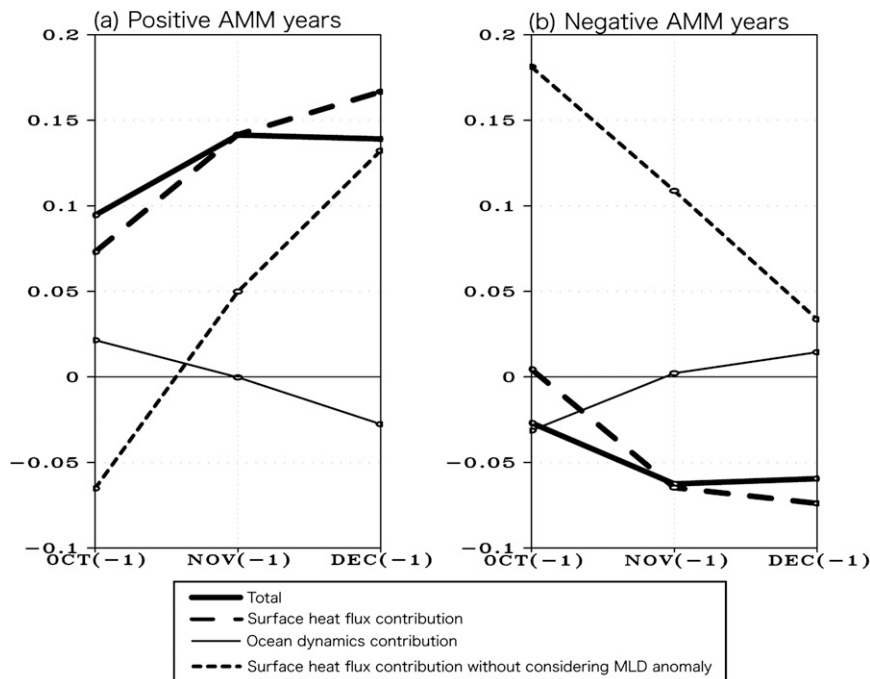


FIG. 9. Rate of change of mixed layer temperature anomaly in the region 5° – 24° N, 36° – 20° W for the (a) positive and (b) negative AMM years (10^{-7} K s^{-1}): rate of change (“Total”) is determined by sea surface heat flux contribution and ocean dynamics contribution. Also shown is sea surface heat flux contribution without considering interannual variation of mixed layer depth. Anomalies above 90% significance level are shown by filled circles.

changes of the simulated GD are most remarkable at around 100 m. Then, we calculate the rate of change of the subsurface temperature at a depth of 106 m and the vertical velocity at a depth of 122 m (Fig. 5). The rate of change is determined by three terms: the vertical heat transport term, the horizontal heat transport term, and the residual term that is computed as the difference between the tendency term and these heat transport terms. The residual term is mostly due to the process of mixing. Also, we assume that the vertical velocity at the depth is composed of local Ekman pumping and the residual (mostly due to remote effects and nonlinear effects) that is calculated by subtracting the Ekman pumping from the model vertical velocity.

The subsurface temperature in Region A decreases from June through September (Fig. 5a). The vertical heat transport related to upwelling dominates the cooling tendency with a peak in August; this is due to the local wind-induced upwelling from June through September (Fig. 5b). We note that the variation of wind stress curl is associated with the meridional migration of the ITCZ (Fig. 4); it is located at the southernmost latitude in boreal spring, then moves northward during late spring, and reaches the northernmost location in summer. The above mechanism of seasonal variation of the GD is consistent with the previous works of Siedler et al. (1992) and Yamagata and

Iizuka (1995), who investigated the annual cycle of the GD from both observations and OGCM outputs.

To quantify the effect of the GD on the overlying SST, the mixed layer heat budget is calculated by

$$\frac{\partial T_{\text{mix}}}{\partial t} = \frac{Q - q_{\text{sw}}}{\rho C_p H_{\text{mix}}} - W_{\text{ent}} \frac{T_{\text{mix}} - T_e}{H_{\text{mix}}} - \mathbf{U} \cdot \nabla T_{\text{mix}} + \text{residual}. \quad (1)$$

Here T_{mix} is the mixed layer temperature, which is a proxy of SST, ρ is the seawater density, C_p the heat capacity of the seawater, and H_{mix} the mixed layer depth, which is calculated as the depth at which the potential density becomes 0.125 kg m^{-3} larger than the surface density. The quantity Q denotes the net sea surface heat flux, and q_{sw} is the downward solar insolation that penetrates through the bottom of the mixed layer. Thus, the first term on the right-hand side represents the influence of atmospheric thermal forcing. The second term on the right-hand side represents the oceanic cooling associated with entrainment for which W_{ent} is the entrainment rate, and T_e is the temperature of water entrained into the mixed layer and taken to be the temperature 5 m below the mixed layer. The third term, $\mathbf{U} \cdot \nabla T_{\text{mix}}$, represents the horizontal heat transport in the mixed layer. Entrainment rate can be assumed by

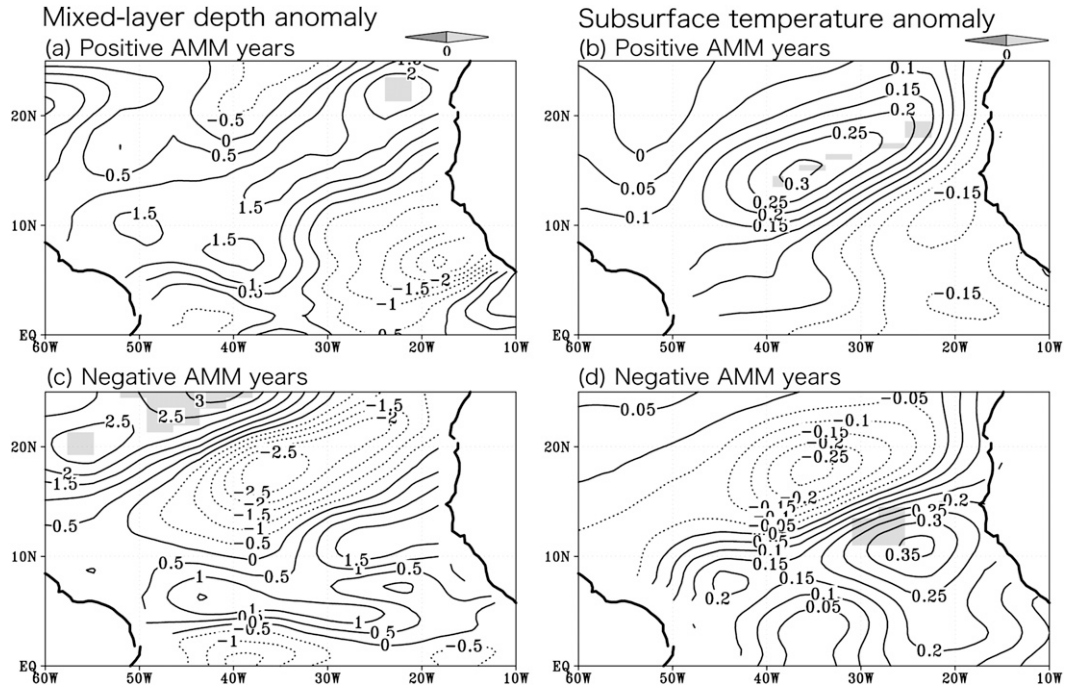


FIG. 10. (a) Mixed layer depth and (b) subsurface temperature anomalies at a depth of 106 m in November of the year before positive AMM. Contour interval for mixed layer depth is 0.5 m, for subsurface temperature is 0.05°C. Light (dark) shading denotes positive (negative) anomalies above 90% significance level. (c),(d) as in (a),(b) but for the negative AMM.

$$W_{\text{ent}} = \frac{\partial H_{\text{mix}}}{\partial t} + W_{\text{mb}} + \mathbf{U} \cdot \nabla H_{\text{mix}}, \quad (2)$$

where $\partial H_{\text{mix}}/\partial t$ denotes the rate of change of the mixed layer depth, W_{mb} is the vertical velocity at the base of the mixed layer, and $\mathbf{U} \cdot \nabla H_{\text{mix}}$ is the horizontal transport. If W_{ent} is negative, we assume $W_{\text{ent}} = 0$.

The climatological rate of change of mixed layer temperature is dominated by the sea surface heat flux contribution from boreal winter through spring, but not from boreal summer through fall (Fig. 5c). During this period the cold-water entrainment cools the mixed layer, which is associated with the intensified upwelling and cold subsurface temperature in the GD region. Figure 6a shows the horizontal distribution of the simultaneous correlation between the climatological rate of change of the mixed layer temperature [the first term in the lhs of Eq. (1)] and the climatological sea surface heat flux contribution [the first term in the rhs of Eq. (1)] from June to September. We assume that the seasonal variation of SST in the region where the correlation is less than 0.9 is influenced by ocean dynamics. Actually, the correlation is lower than 0.9 in the equatorial region, near northeastern Brazil and the GD region. It is well known that the mixed layer temperature in the equatorial region is influenced by ocean processes. Also, the

low correlation near northeastern Brazil may be linked with the strong meridional heat transport associated with the western boundary current: the North Brazil Current. Here, we find that the ocean processes are important in the GD region. However, Fig. 6b shows that the role of ocean processes is reduced from October to May when upwelling does not occur, as shown in Fig. 5b. The cold-water entrainment associated with upwelling during summer provides a favorable field for more heat absorption from the atmosphere because of the reduced mixed layer temperature. Therefore, it is very important to reproduce the variability of the subsurface GD for a realistic simulation of the seasonal variation of SST there, especially in summer. The present result is supported by the previous observational data analysis of Yu et al. (2006).

4. The Atlantic meridional mode

To begin the present section, we have applied an empirical orthogonal function (EOF) analysis to the model SSTA. The first mode explains 34% of the total variance, which corresponds to the Atlantic El Niño (Zebiak 1993). The second mode captures the meridional SST gradient across the equator, which explains 10% of the total variance (figure not shown). This situation is consistent with the analysis of ERSSTv2, in which the

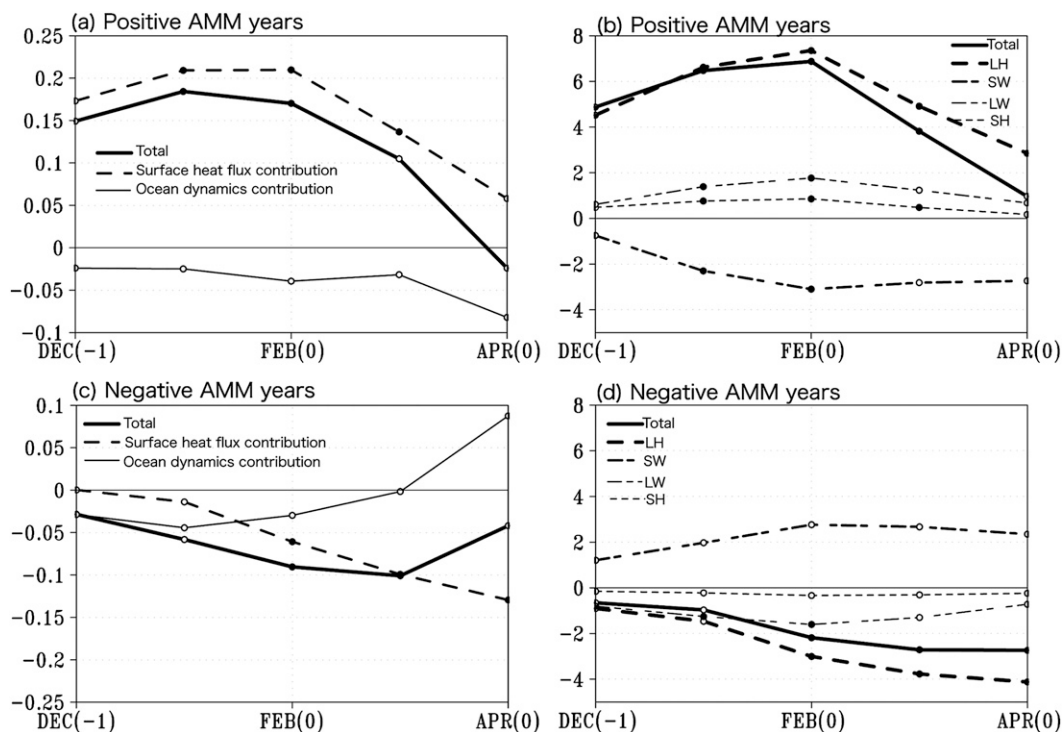


FIG. 11. (a) Rate of change of mixed layer temperature anomaly in the region $5^{\circ}\text{--}15^{\circ}\text{N}$, $50^{\circ}\text{--}20^{\circ}\text{W}$ for the positive AMM years (10^{-7} K s^{-1}): rate of change (“Total”) is determined by sea surface heat flux contribution and ocean dynamics contribution. (b) Anomalous sea surface heat flux in the region $5^{\circ}\text{--}15^{\circ}\text{N}$, $50^{\circ}\text{--}20^{\circ}\text{W}$ for the positive AMM years (W m^{-2}): net sea surface heat flux (“Total”) is determined by latent heat flux (LH), shortwave radiation (SW), longwave radiation (LW), and sensible heat flux (SH). Anomalies above 90% significance level are shown by filled circles. (c),(d) as in (a),(b) but for the negative AMM years.

first (second) mode corresponds to the Atlantic El Niño (AMM), and its variance contribution is 28% (21%). Hence, the model has good skill in reproducing the dominant modes of climate variability in the tropical Atlantic.

Hereafter, we define the AMM index (AMMI) (e.g., Doi et al. 2009) as the difference between the northern index (SSTA in $5^{\circ}\text{--}15^{\circ}\text{N}$, $50^{\circ}\text{--}20^{\circ}\text{W}$) and the southern index (SSTA in $5^{\circ}\text{--}15^{\circ}\text{S}$, $20^{\circ}\text{W--}10^{\circ}\text{E}$). As shown in Figs. 7a and 7b, the model simulates the observed variability rather well. In particular, the phase locking to boreal spring is simulated well even though the simulated standard deviation is 0.34°C , which is about 70% of the observation. We note that the simulated index has another peak in boreal fall, which cannot be identified in the observation. This may be linked with a too strong Atlantic Niño-2, which has a peak in November–December (Okumura and Xie 2006). In this study, we focus on the stronger peak in boreal spring. We further introduce the spring AMMI by averaging the AMMI from March to May, as shown in Fig. 7c. We adopt a composite analysis to clarify the mechanism of the AMM. Here, we select 10 typical positive years with the warm (cold) SSTA in the Northern (Southern) Hemisphere, and 10 typical

negative years with the cold (warm) SSTA in the Northern (Southern) Hemisphere. The spring AMMI in those years exceeds one standard deviation.

a. Composites for positive events

The warm SSTA first appears in the eastern North Atlantic during early winter of the previous year (Fig. 8a). It may be linked with the interannual variability of the GD there. To examine this possibility, we have calculated the mixed layer heat budget anomaly in the positive SSTA region ($5^{\circ}\text{--}24^{\circ}\text{N}$, $36^{\circ}\text{--}20^{\circ}\text{W}$; see Fig. 8a). As shown in Fig. 9a, the rate of change of the mixed layer temperature anomaly is positive during late fall of the previous year. This warming tendency is mainly due to the sea surface heat flux contribution (thick dashed line in Fig. 9a), and not ocean dynamics (heat transport and diffusion terms), which is computed as the difference between the tendency term and the sea surface heat flux contribution. We note that the anomaly of the sea surface heat flux contribution includes interannual variability of both the sea surface heat flux and the mixed layer depth [see the first term in the rhs of Eq. (1)]. To show the importance of the anomalous interannual variation of the mixed layer

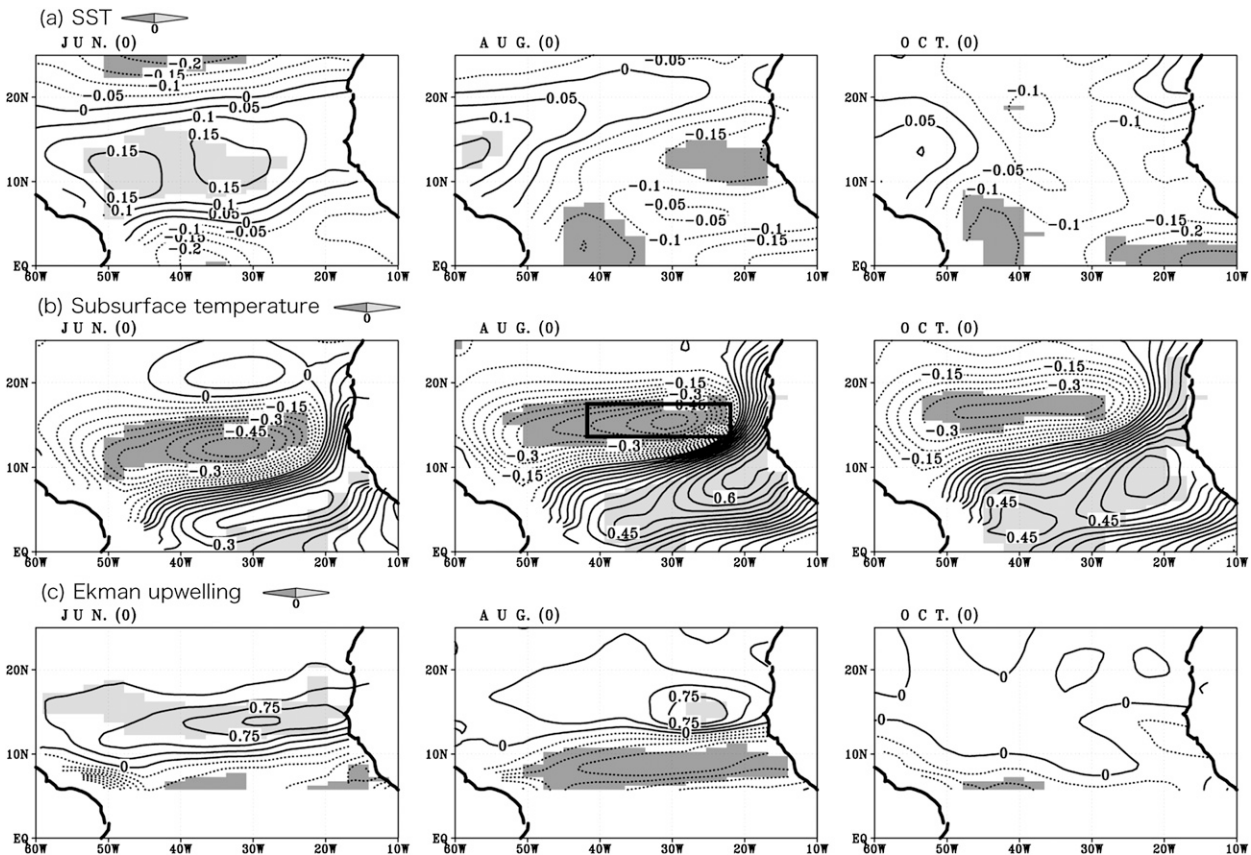


FIG. 12. Anomalous (a) SST, (b) subsurface temperature at a depth of 106 m, and (c) Ekman upwelling for the positive AMM years: Contour interval for SST and subsurface temperature 0.05°C ; for Ekman upwelling $0.25 \times 10^{-6} \text{ m s}^{-1}$. Light (dark) shading denotes positive (negative) anomalies above 90% significance level. Location of Region A is also shown for August (0) in (b).

depth, we have recalculated the anomalous sea surface heat flux contribution term using the climatological mixed layer depth. This is shown as the “surface heat flux contribution without considering MDL anomaly” (thin broken line in Fig. 9). If we do not take into account the interannual variation in the mixed layer depth, the contribution from the sea surface heat flux cannot explain the anomalous warming tendency of the mixed layer temperature (e.g., Morioka et al. 2009, manuscript submitted to *Climate Dyn.*). Therefore, we can conclude that the interannual variability of the mixed layer depth is crucial for the preconditioning phase of the AMM.

In the GD region during November of the previous year, the anomalously deep mixed layer depth associated with anomalously warm subsurface temperature is seen in Figs. 10a and 10b. This situation reduces the sensitivity of the mixed layer temperature to the seasonal atmospheric cooling in November (e.g., Fig. 5c). As a result, the positive SSTA appears in early winter. The precondition of the AMM associated with the GD, as discussed here, is very important for improving the prediction skill of the AMM. However, all previous

works have neglected the in situ role of the GD in the precondition of the AMM and focused only on the remote effects of the ENSO and the North Atlantic Oscillation through the atmospheric bridge (Xie and Carton 2004, for a recent review).

The positive SSTA in early winter develops from winter through spring and matures in late spring (Fig. 8a). To understand the mechanism in detail, we have calculated the mixed layer heat balance anomaly in the region for the northern index of AMMI (see the right panel of Fig. 8a for the location). As shown in Fig. 11a, the rate of change of the mixed layer temperature anomaly is positive from December in the previous year to March with a maximum in January. This warming tendency is mainly due to the weakened latent heat loss in the surface heat flux anomaly (Fig. 11b). The meridional gradient associated with the positive SSTA in the northern tropics leads to the anomalously northward migration of the ITCZ. This generates the southwesterly wind anomaly and weaker trade winds there, as shown in Fig. 8c. As a result, the latent heat loss due to evaporation is reduced (Fig. 8b). This leads to even warmer SSTA and

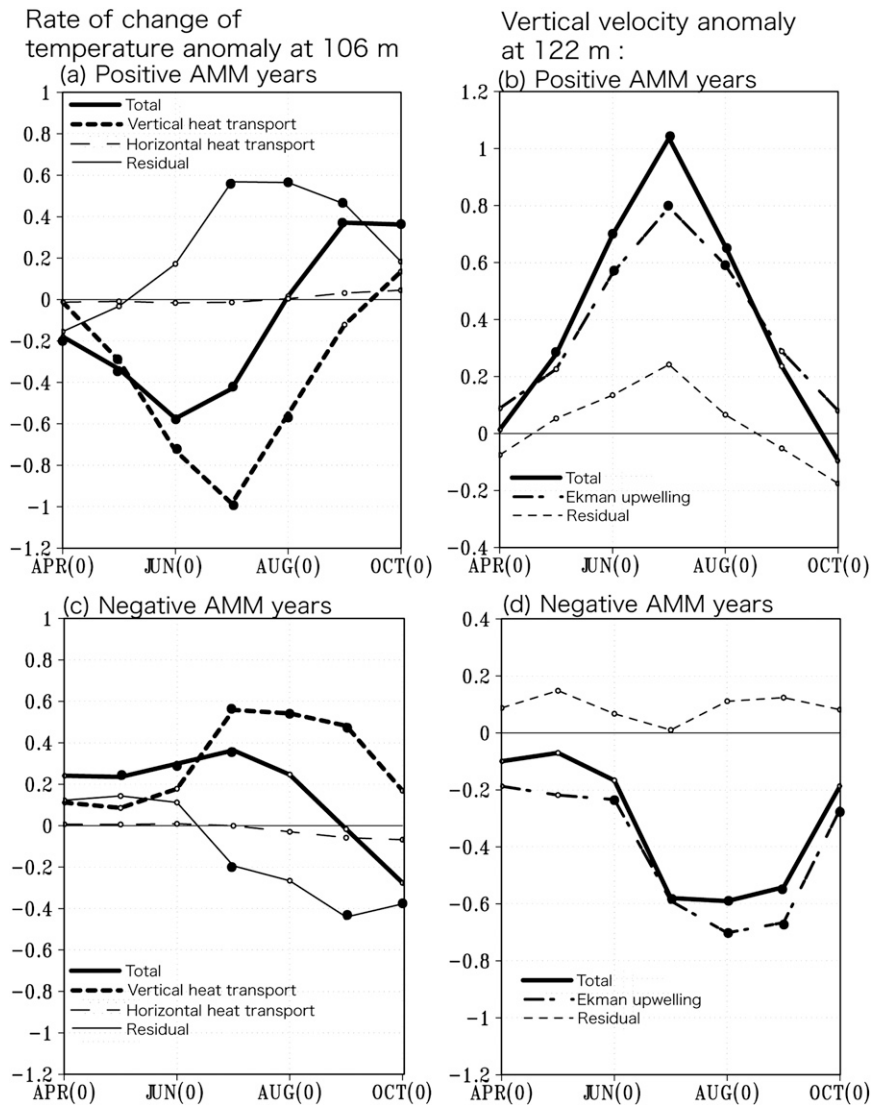


FIG. 13. Same as Fig. 5a, but for rate of change of temperature anomaly in the positive AMM years. (b) Same as Fig. 5b, but for vertical velocity anomaly in the positive AMM years. Anomalies above 90% significance level are shown by filled circles. (c),(d) as in (a),(b) but for the negative AMM years.

causes farther northward migration of the ITCZ. The above positive feedback process is consistent with that in previous work (Carton et al. 1996; Chang et al. 1997; Xie 1999), and the recent work of Huang and Shukla (2005) based on another CGCM.

As shown in Fig. 12a, the positive SSTA in the northern tropics decays suddenly in summer and disappears in fall, particularly on the eastern side of the North Atlantic. This zonal asymmetry in the decay process may also be linked with the dome there. The subsurface temperature in the GD region cools anomalously, reaching a maximum in fall (Fig. 12b). Figure 13a shows the heat balance for the subsurface temperature anomaly at a

depth of 106 m. The rate of change of subsurface temperature anomaly in Region A is negative from April through August with a maximum in June. This cooling tendency is mainly due to the vertical heat transport related to anomalously strong local Ekman upwelling owing to the positive wind stress curl anomaly (Fig. 13b). The anomalously northward migration of the ITCZ from spring to summer is responsible for this, as shown in Fig. 12c. The “unraveled” linkage is also supported by assimilation data (Ruiz-Barradas et al. 2000), a simple ocean model (Joyce et al. 2004), a simple coupled model (Lee and Wang 2008), and OGCM results forced by reanalysis winds (Doi et al. 2009).

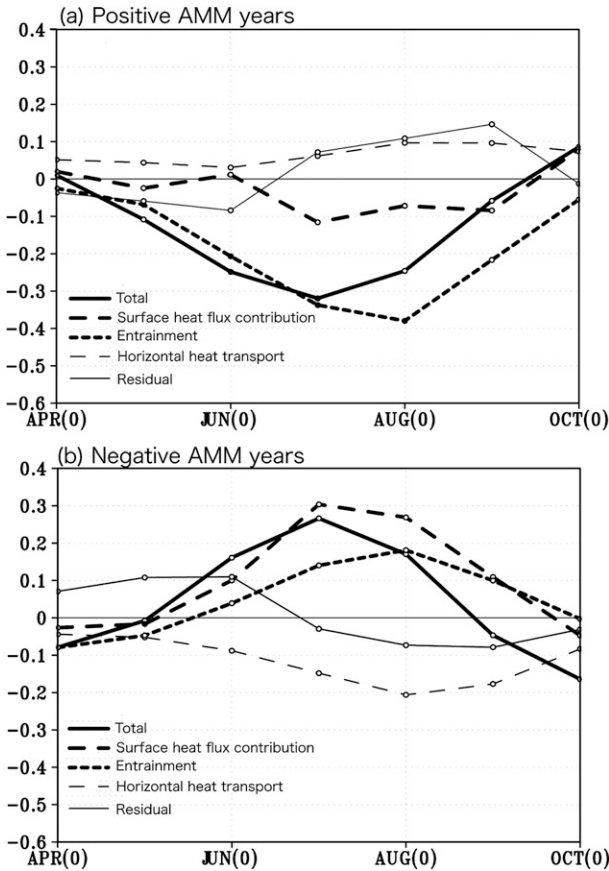


FIG. 14. As in Fig. 5c but for anomalies in the (a) positive and (b) negative AMM years. Anomalies above 90% significance level are shown by filled circles.

To examine the role of the subsurface GD in the decay phase of the warm SSTA, we have calculated composites of the mixed layer heat budget anomaly over Region A (Fig. 14a). The mixed layer temperature anomaly decays from May to September owing to the intensified entrainment cooling. This is associated with anomalously strong upwelling, which induces the anomalous cooling of the GD during this season. The intensified entrainment rate is not due to the wind speed anomaly because the wind speed is weakened associated with the WES feedback; it is due to stronger Ekman upwelling associated with the anomalously northward migration of the ITCZ. The importance of ocean dynamics in the GD region is confirmed by the weaker correlation between the rate of change of the mixed layer temperature anomaly and the sea surface heat flux contribution anomaly in boreal summer, as shown in Fig. 15a. Thus, the ocean dynamics in the GD cannot be neglected to explain the decay of the AMM, especially in the northeastern tropical Atlantic. This mechanism is also supported by the OGCM results of Doi et al. (2009), who showed the im-

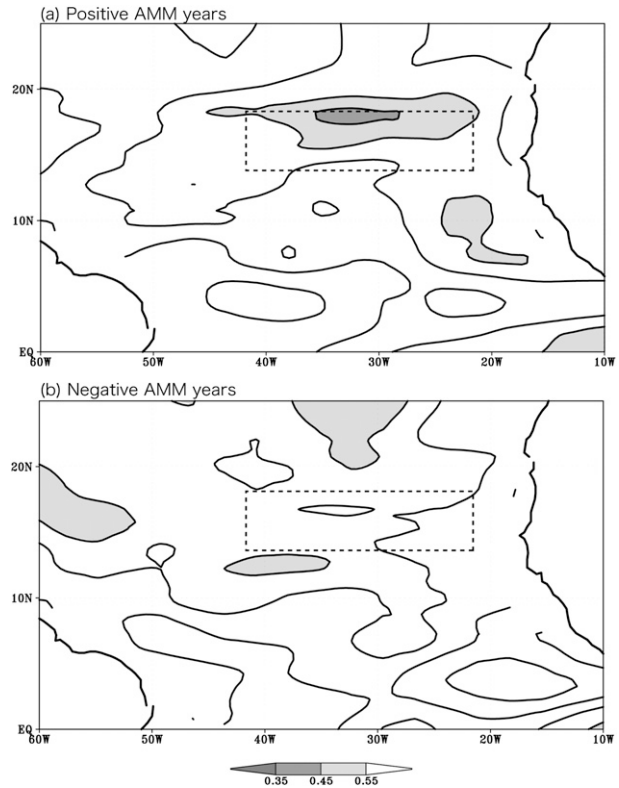


FIG. 15. Correlation between the rate of change of mixed layer temperature anomaly and the sea surface heat flux contribution anomaly from June to September in the (a) positive and (b) negative AMM years: Contour interval 0.1; values lower than 0.55 shaded. Location of Region A (14° – 18° N, 42° – 22° W) is shown by dashed line.

portance of the vertical heat transport during the decay of the AMM by calculating the heat budget anomaly in the upper 58 m. Joyce et al. (2004), using a 1.5-layer model, and Lee and Wang (2008), using a simple coupled model, claimed that the horizontal heat transport is important for the decay of the AMM. The horizontal heat transport is very effective in the western boundary region. However, in the GD region, the vertical heat transport through entrainment is more dominant than the horizontal heat transport, as shown in Fig. 14a. The weak horizontal temperature gradient in the GD region may explain the difference (see Foltz and McPhaden 2006).

b. Composites for negative events

In the negative AMM years, the cold SSTA in the Northern Hemisphere appears in the northeastern tropical Atlantic during early winter, develops from late winter to early spring, and peaks in spring. This is close to a mirror image of the positive years (Fig. 16a). From the analysis of the heat balance in the mixed layer during early winter of the previous year in the negative SSTA

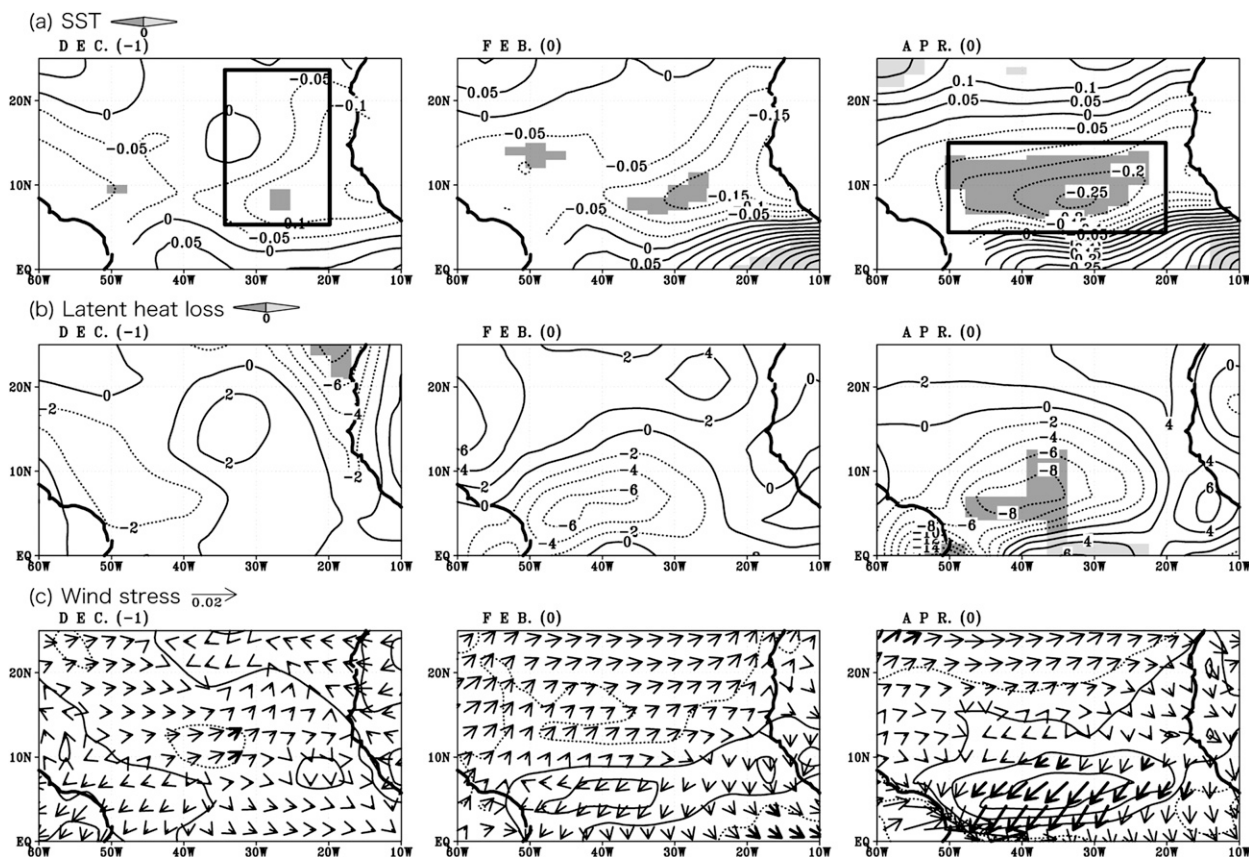


FIG. 16. As in Fig. 8 but for the negative AMM years.

region (5°–24°N, 36°–20°W; see Fig. 16a), we find that the initial cooling tendency is linked closely to the contribution from the sea surface heat flux, not to ocean dynamics contribution (Fig. 9b). Because the mixed layer is anomalously shallow in association with the stronger GD in November of the previous year, as shown in Figs. 10c,d, the sensitivity of the climatological atmospheric cooling to the mixed layer temperature is enhanced. This leads to the negative SSTa in the northeastern tropical Atlantic.

The cold SSTa in early winter is further cooled during spring. This cooling tendency is mainly due to anomalously strong latent heat loss (Figs. 11c and 11d). During the same season, we find anomalously southward migration of the ITCZ and the northeasterly wind anomaly in the Northern Hemisphere, as seen in Fig. 16c. This, in turn, leads to weaker Ekman upwelling in the GD region and results in the warmer dome in the following fall through positive vertical heat transport anomaly (Figs. 13c,d and 17b). Thus, the mechanism for preconditioning and the subsequent evolution in the negative AMM years is almost a mirror image of those in the positive AMM years.

The cold mixed layer temperature anomaly in the northern tropics weakens during boreal summer owing

to anomalous warming both by sea surface heat flux and the weakened cold-water entrainment (Fig. 14b). This is also supported by mapping the correlation between the rate of change of mixed layer temperature anomaly and the contribution from the sea surface heat flux during summer, as seen in Fig. 15b. The correlation in the GD region is not as high as that in the surrounding region, suggesting that the negative AMM is also influenced by the ocean dynamics in the GD region. However, we note that the correlation is higher by about 0.2 than that in the positive AMM years, which suggests that the ocean dynamics may be less efficient in affecting the mixed layer temperature in the negative AMM years. It may be explained by the anomalously deep mixed layer associated with the cold SSTa in the northern tropics during spring. Since the mixed layer becomes thin in association with the decay of the cold SSTa during boreal summer, the efficiency of entrainment weakens.

5. Summary and discussions

Using outputs from the CGCM that simulates the tropical oceanic conditions in the Atlantic rather well, we

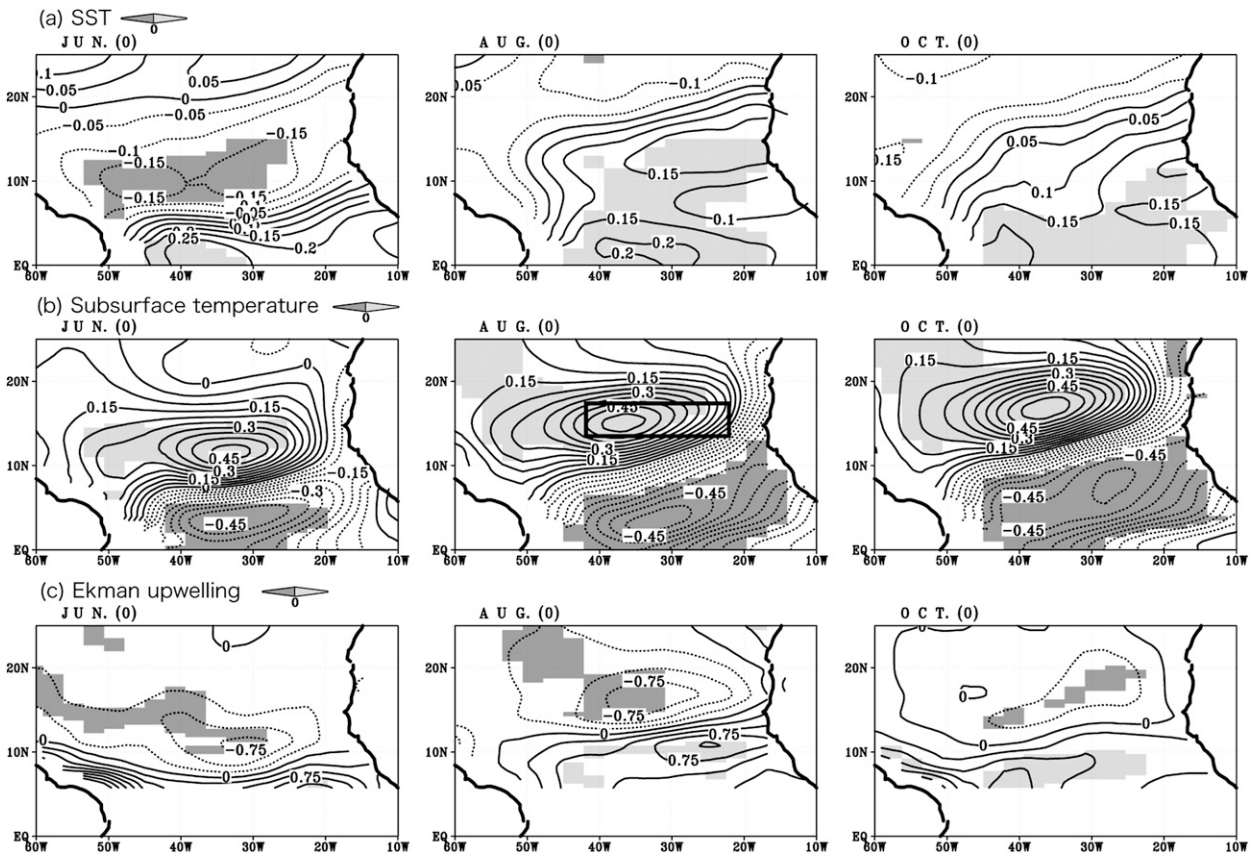


FIG. 17. As in Fig. 12 but for the negative AMM years.

have examined the air–sea coupled variability associated with the Guinea Dome. The GD develops off Dakar from late spring to late fall owing to wind-induced Ekman upwelling associated with the northward migration of the ITCZ. This seasonal evolution of the upwelling provides a favorable field for absorbing heat from the atmosphere during summer in GD region because of the cool mixed layer temperature through the cold-water entrainment. Therefore, it is very important to reproduce the variability of the subsurface temperature to simulate the seasonal cycle of the SST in the GD region.

We have found a remarkable link between the AMM and the interannual modulation in the seasonal variation of the GD. Our conclusion is summarized schematically in Fig. 18. During the preconditioning phase of the AMM, the GD is anomalously weak (strong) and the mixed layer is anomalously deep (shallow) in the GD region in November of the previous year. This condition reduces (enhances) the sensitivity of the mixed layer temperature to atmospheric cooling, leading to the weak positive (negative) SSTA in early winter. This weak anomaly is amplified and then sustained in the following spring through the WES positive feedback associated with the

ITCZ migration; anomalously northward (southward) migration of the ITCZ causes the southwesterly (northeasterly) wind anomaly in the northern tropics and weaker (stronger) trade winds. This results in less (more) evaporation and thus suppressed (intensified) latent heat loss, leading to warmer (colder) SSTA in the Northern Hemisphere. The outcome is farther northward (southward) migration of the ITCZ. Here, we find the existence of an active ocean–atmosphere feedback mechanism. When the ITCZ is located anomalously north (south) from late spring to early summer, the GD becomes unusually cold (warm) as a result of stronger (weaker) upwelling associated with the positive (negative) wind stress curl anomaly. This situation may be interpreted as a strengthened (weakened) annual cycle. The stronger (weaker) entrainment cooling associated with upwelling (downwelling) anomaly plays an important role in the decay of the warm (cold) SSTA in the GD region during summer as a negative feedback. Also, the AMM is expected to have a biennial nature since both positive and negative AMM events are linked with the GD as an almost mirror image. As shown in Fig. 7c, some strong events of the AMM are followed by opposite events,

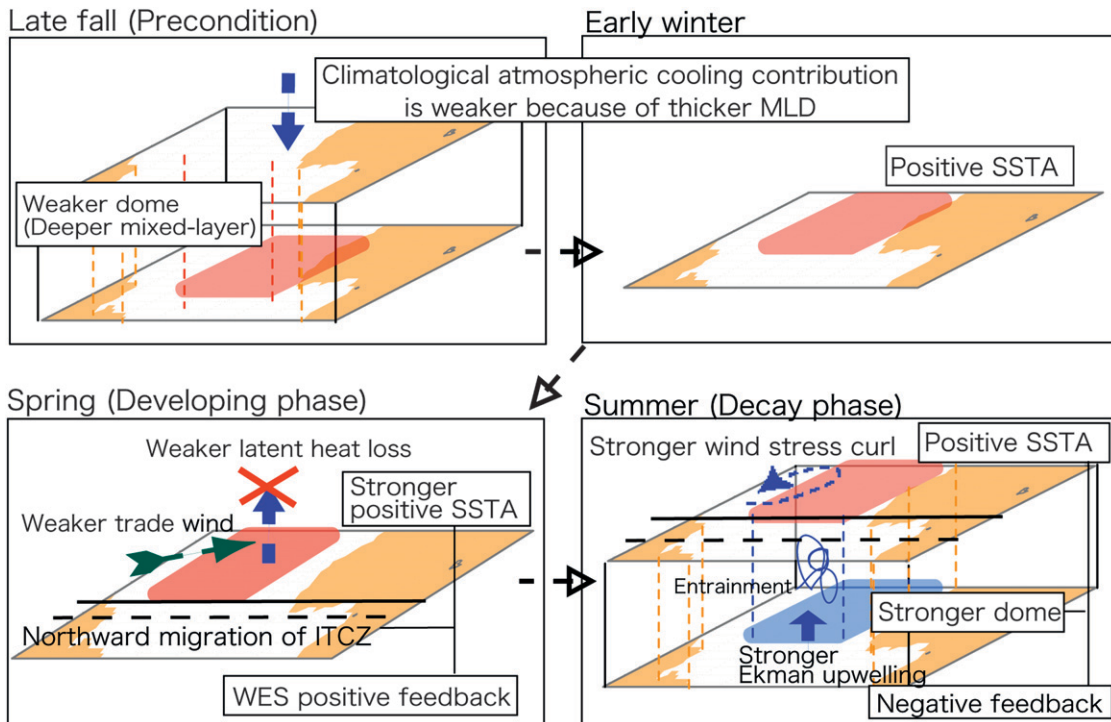


FIG. 18. Schematic diagram of the positive AMM and its link with the GD. Late fall in the preconditioning phase of the AMM: the GD is anomalously weak and the mixed layer is anomalously deep in the GD region. This condition reduces the sensitivity of the mixed layer temperature to the atmospheric cooling, and as a result leading to the positive SSTA in early winter. Spring: this situation is amplified and sustained by the WES feedback through the ITCZ migration; anomalously northward migration of the ITCZ causes the southwesterly wind anomaly in the Northern Hemisphere and weaker trade winds. This results in weaker evaporation and thus suppressed latent heat loss, leading to warmer SSTA. The outcome is farther northward migration of the ITCZ. Summer: the GD becomes unusually cold as a result of stronger Ekman upwelling associated with the positive wind stress curl anomaly owing to anomalously northward migration of the ITCZ. It plays an important role on the decay of the warm SSTA through entrainment as a negative feedback.

although the power spectrum of the AMMI does not show a significant peak at the biennial period.

We show for the first time that the preconditioning phase of the AMM is associated with the interannual variation of the GD. We note that some previous works suggested that the preconditioning phase of the AMM is influenced by the ENSO or the North Atlantic Oscillation [see Xie and Carton (2004) for a recent review on the AMM]. The composite of SSTA in the positive (negative) AMM years shows a weak El Niño (La Niña) in the Pacific in our model. In fact, the 10 positive (negative) AMM years include four positive and two negative events (one positive and two negative events) of ENSO. In the observation period that we analyzed, eight positive (10 negative) AMM years include three (one) El Niño and no (three) La Niña years. The ENSO may partly influence the preconditioning phase, but the significance level is too low to confirm this. We need further study to estimate the relative importance between the local coupled process linked with the GD and the remote influence from ENSO.

The AMM is sometimes interpreted as part of a tri-pole pattern of SSTA over the North Atlantic associated with the North Atlantic Oscillation (Seager et al. 2000; Ruiz-Barradas et al. 2000). In addition, Xie and Tanimoto (1998) suggested a Pan-Atlantic pattern, with bands of alternating signs of SSTA from the South Atlantic to Greenland on the decadal time scale. Because the tropical Atlantic SST variability influences the North Atlantic atmosphere and ocean (Watanabe and Kimoto 1999), the Guinea Dome region may be important to understand the connection between the tropics and the extratropics. In fact, the 10 positive (negative) AMM years include a few events of the North Atlantic Oscillation; two positive and three negative events (one positive and one negative event). In the observation, 8 positive (10 negative) AMM years include one (two) positive NAO events. However, the composite fields in our model do not show a clear sign associated with the North Atlantic Oscillation.

Most previous studies on the AMM focused only on the atmospheric forcing of the SSTA and paid little attention to how the oceanic subsurface temperature

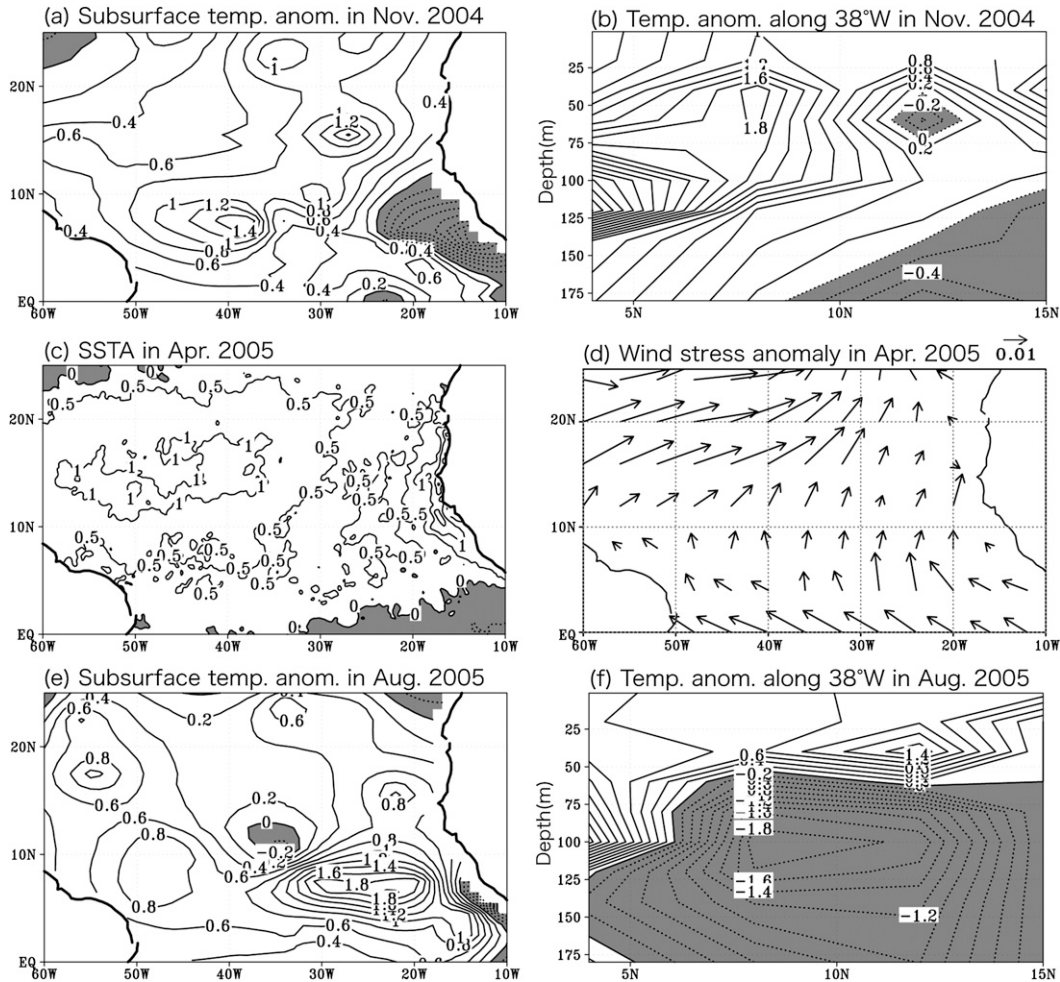


FIG. 19. (a) Subsurface temperature anomaly at a depth of 50 m (Argo) and (b) vertical profile of temperature anomaly along 38°W (PIRATA) in November 2004 (°C); contour interval 0.2°C; negative anomalies shaded. (c) SSTA (°C) in April 2005 (VIRS); contour interval 0.5°C; Negative anomalies shaded. (d) Wind stress anomaly ($N m^{-2}$) (QuickSCAT) in April 2005. (e),(f) as in (a),(b) but for August 2005.

influences the SST in the GD region. However, as we have discussed here, the coupled variability between the AMM and the oceanic upwelling dome is very important and needs to be addressed more. Further research along this line will contribute to improvement in predictability of the AMM. Particularly, both the preconditioning and decay phases need to be explored more. As the sustained AMM in summer is significantly linked with the activity of hurricanes originated in the northern tropical Atlantic (Kossin and Vimont 2007; Vimont and Kossin 2007), the research in the negative feedback associated with the upwelling dome is of great importance from an economic as well as societal viewpoint. Present results, despite several supporting evidences in the observation, are mostly based on our CGCM outputs. It is rather difficult to compare those with the observation to a full extent because of lack of systematic oceanic measure-

ments in the key region of the tropical Atlantic. However, the observational efforts such as the Prediction and Research Moored Array in the Atlantic (PIRATA) and Argo are improving the situation. As an example, the positive AMM in 2005 is shown in Fig. 19. The northern tropical Atlantic was preconditioned with the anomalously warm subsurface temperature in November 2004 (Figs. 19a and 19b). Then, the positive AMM associated with the northward migration of the ITCZ developed in April 2005 (Figs. 19c and 19d), and then decayed because of the anomalously strong GD in August 2005 (Figs. 19e and 19f). These observations support the ocean-atmosphere coupled scenario developed in the present paper. More systematic ocean-atmosphere observations in the relevant region will lead to further understanding of the climate variability in the tropical Atlantic as well as improving prediction skills by use of a CGCM.

Acknowledgments. We thank Drs. Hisashi Nakamura and Shang-Ping Xie for helpful comments and suggestions. The present research is supported by the Japan Society for Promotion of Science (JSPS) through both Grant-in-Aid for Scientific Research B (20340125). Also, the first author is supported by the Research Fellowship of the JSPS for Young Scientists (208479). Wavelet software was provided by C. Torrence and G. Compo, and is available online (<http://atoc.colorado.edu/research/wavelets/>). VIRS SST was produced and supplied by the Earth Observation Research Center, Japan Aerospace Exploration Agency. UTCM was run on the HITACHI SR11000/J1 of the Information Technology Center, the University of Tokyo under the cooperative research with Center for Climate System Research, the University of Tokyo. We acknowledge the modeling groups, the Program for Climate Model Diagnosis and Intercomparison (PCMDI), and the WCRP's Working Group on Coupled Modelling (WGCM) for their roles in making available the WCRP CMIP3 multimodel dataset. Support of this dataset is provided by the Office of Science, U.S. Department of Energy.

REFERENCES

- Bourles, B., and Coauthors, 2008: The PIRATA program: History, accomplishments, and future directions. *Bull. Amer. Meteor. Soc.*, **89**, 1111–1125.
- Breugem, W.-P., P. Chang, C. J. Jang, J. Mignot, and W. Hazeleger, 2008: Barrier layers and tropical Atlantic SST biases in coupled GCMs. *Tellus*, **60A**, 885–897.
- Carton, J. A., X. Cao, B. S. Giese, and A. M. da Silva, 1996: Decadal and interannual SST variability in the tropical Atlantic Ocean. *J. Phys. Oceanogr.*, **26**, 1165–1175.
- Chakraborty, A., T. Tozuka, T. Miyasaka, M. Mujumdar, S. K. Behera, and T. Yamagata, 2003: Development of the University of Tokyo Community Model (UTCM) for climate system: Preliminary results. Tech. Rep. for Mitsubishi Heavy Industries, 49 pp.
- , S. K. Behera, M. Mujumdar, R. Ohba, and T. Yamagata, 2006: Diagnosis of tropospheric moisture over Saudi Arabia and influences of IOD and ENSO. *Mon. Wea. Rev.*, **134**, 598–617.
- Chang, P., L. Ji, and H. Li, 1997: A decadal climate variation in the tropical Atlantic ocean from thermodynamic air-sea interactions. *Nature*, **385**, 516–518.
- Conkright, M. E., and Coauthors, 1998: World Ocean Database 1998 documentation and quality control. National Oceanographic Data Center Rep., 16 pp.
- Davey, M. K., and Coauthors, 2002: STOIC: A study of coupled model climatology and variability in tropical ocean regions. *Climate Dyn.*, **18**, 403–420.
- Doi, T., T. Tozuka, and T. Yamagata, 2009: Interannual variability of the Guinea Dome and its possible link with the Atlantic Meridional Mode. *Climate Dyn.*, **33**, 985–998.
- Foltz, G. R., and M. J. McPhaden, 2006: The role of oceanic heat advection in the evolutions of tropical north and south Atlantic SST anomalies. *J. Climate*, **19**, 6122–6138.
- Gent, P. R., and J. C. McWilliams, 1990: Isopycnal mixing in ocean circulation models. *J. Phys. Oceanogr.*, **20**, 150–155.
- Guan, Z., S. Iizuka, M. Chiba, S. Yamane, K. Ashok, M. Honda, and T. Yamagata, 2000: Frontier Atmospheric General Circulation Model version 1.0 (FrAM1.0): Model climatology. Tech. Rep. FTR-1, 27 pp.
- Hazeleger, W., and R. J. Haarsma, 2005: Sensitivity of tropical Atlantic climate to mixing in a coupled ocean-atmosphere model. *Climate Dyn.*, **25**, 387–399.
- Hu, Z.-Z., B. Huang, and K. Pegion, 2008: Leading patterns of the tropical Atlantic variability in a coupled general circulation model. *Climate Dyn.*, **30**, 703–726.
- Huang, B., and J. Shukla, 2005: Ocean-atmosphere interactions in the tropical and subtropical Atlantic ocean. *J. Climate*, **18**, 1652–1672.
- Joyce, T. M., C. Frankignoul, J. Yang, and H. E. Phillips, 2004: Ocean response and feedback to the SST dipole in the tropical Atlantic. *J. Phys. Oceanogr.*, **34**, 2525–2540.
- Kossin, J. P., and D. J. Vimont, 2007: A more general framework for understanding Atlantic hurricane variability and trends. *Bull. Amer. Meteor. Soc.*, **88**, 1767–1781.
- Kubota, M., N. Iwasaka, S. Kizu, M. Konda, and K. Kutsuwada, 2002: Japanese ocean flux data sets with use of remote sensing observations (J-OFURO). *J. Oceanogr.*, **58**, 213–225.
- Kuo, H., 1974: Further studies of the parameterization of the influence of cumulus convection on large-scale flow. *J. Atmos. Sci.*, **31**, 1232–1240.
- Kushnir, Y., W. A. Robinson, P. Chang, and A. W. Robertson, 2006: The physical basis for predicting Atlantic sector seasonal to interannual climate variability. *J. Climate*, **19**, 5949–5970.
- Lee, S.-K., and C. Wang, 2008: Tropical Atlantic decadal oscillation and its impact on the equatorial atmosphere-ocean dynamics: A simple model study. *J. Phys. Oceanogr.*, **38**, 193–212.
- Mazeika, P. A., 1967: Thermal domes in the eastern tropical Atlantic Ocean. *Limnol. Oceanogr.*, **12**, 537–539.
- Meehl, G. A., C. Covey, T. Delworth, M. Latif, B. McAvaney, J. F. B. Mitchell, R. J. Stouffer, and K. E. Taylor, 2007: The WCRP CMIP3 multimodel dataset: A new era in climate change research. *Bull. Amer. Meteor. Soc.*, **88**, 1383–1394.
- Okumura, Y., and S. P. Xie, 2006: Some overlooked features of tropical Atlantic climate leading to a new Niño-like phenomenon. *J. Climate*, **19**, 5859–5874.
- Pacanowski, R. C., and S. G. H. Philander, 1981: Parameterization of vertical mixing in numerical models of tropical oceans. *J. Phys. Oceanogr.*, **11**, 1443–1451.
- , and S. M. Griffies, 2000: MOM 3.0 manual. NOAA/GFDL, 680 pp.
- Philander, S. G. H., and R. C. Pacanowski, 1981: The oceanic response to cross-equatorial winds (with application to coastal upwelling in low latitudes). *Tellus*, **33**, 201–210.
- Richter, I., and S. P. Xie, 2008: On the origin of equatorial Atlantic biases in coupled general circulation models. *Climate Dyn.*, **31**, 587–598.
- Rosignol, M., and A. M. Meyrueis, 1964: Campagnes océanographiques du Gerad-Treca. Centre de Recherches Océanographique, Dakar-Thiaroye, ORSTOM, 53 pp.
- Ruiz-Barradas, A., J. A. Carton, and S. Nigam, 2000: Structure of interannual-to-decadal climate variability in the tropical Atlantic sector. *J. Climate*, **13**, 3285–3297.
- Seager, R., Y. Kushnir, M. Visbeck, N. Naik, J. Miller, G. Krahnmann, and H. Cullen, 2000: Causes of Atlantic Ocean climate variability between 1958 and 1998. *J. Climate*, **11**, 165–188.

- Servain, J., 1991: Simple climatic indices for the tropical Atlantic Ocean and some applications. *J. Geophys. Res.*, **96**, 15 137–15 146.
- Siedler, G., N. Zangenberg, and R. Onken, 1992: Seasonal changes in the tropical Atlantic circulation: Observation and simulation of the Guinea Dome. *J. Geophys. Res.*, **97**, 703–715.
- Smagorinsky, J., 1963: General circulation experiments with the primitive equations. 1. The basic experiment. *Mon. Wea. Rev.*, **91**, 99–164.
- Smith, T. M., and R. W. Reynolds, 2004: Improved extended reconstruction of SST (1854–1997). *J. Climate*, **17**, 2466–2477.
- Stockdale, T. N., M. A. Balmaseda, and A. Vidard, 2006: Tropical Atlantic SST prediction with coupled ocean–atmosphere GCMs. *J. Climate*, **19**, 6047–6061.
- Torrence, C., and G. P. Compo, 1998: A practical guide to wavelet analysis. *Bull. Amer. Meteor. Soc.*, **79**, 61–78.
- Tozuka, T., T. Miyasaka, A. Chakraborty, M. Mujumdar, S. K. Behera, Y. Masumoto, H. Nakamura, and T. Yamagata, 2006: University of Tokyo Coupled General Circulation Mode (UTCM1.0). University of Tokyo, Ocean–Atmosphere Research Rep. 7, 44 pp.
- Vimont, D. J., and J. P. Kossin, 2007: The Atlantic Meridional Mode and hurricane activity. *Geophys. Res. Lett.*, **34**, L07709, doi:10.1029/2007GL029683.
- Viterbo, P., and A. C. Beljaars, 1995: An improved land surface parameterization scheme in the ECMWF model and its validation. *J. Climate*, **8**, 2716–2748.
- Watanabe, M., and M. Kimoto, 1999: Tropical-extratropical connection in the Atlantic atmosphere–ocean variability. *Geophys. Res. Lett.*, **26**, 2247–2250.
- Xie, L., T. Yan, and L. Pietrafesa, 2005: The effect of Atlantic sea surface temperature dipole mode on hurricanes: Implications for the 2004 Atlantic hurricanes season. *Geophys. Res. Lett.*, **32**, L03701, doi:10.1029/2004GL021702.
- Xie, P., and P. A. Arkin, 1997: Global precipitation: A 17-year monthly analysis based on gauge observations, satellite estimates, and numerical model outputs. *Bull. Amer. Meteor. Soc.*, **78**, 2539–2558.
- Xie, S.-P., 1999: A dynamic ocean–atmosphere model of the tropical Atlantic decadal variability. *J. Climate*, **12**, 64–70.
- , and Y. Tanimoto, 1998: A pan-Atlantic decadal climate oscillation. *Geophys. Res. Lett.*, **25**, 2185–2188.
- , and J. A. Carton, 2004: Tropical Atlantic variability: Patterns, mechanisms, and impacts. *Earth's Climate: The Ocean–Atmosphere Interaction: From Basin to Global Scales*, *Geophys. Monogr.*, Vol. 147, Amer. Geophys. Union, 121–142.
- Yamagata, T., and S. Iizuka, 1995: Simulation of the tropical thermal domes in the Atlantic: A seasonal cycle. *J. Phys. Oceanogr.*, **25**, 2129–2140.
- Yu, L., X. Jin, and R. A. Weller, 2006: Role of net surface heat flux in seasonal variations of sea surface temperature in the tropical Atlantic Ocean. *J. Climate*, **19**, 6153–6169.
- Zebiak, S. E., 1993: Air–sea interaction in the equatorial Atlantic region. *J. Climate*, **6**, 1567–1586.